III

THE RADON TRANSFORM AND ITS APPLICATIONS

BY

HARRISON H. BARRETT

*Department of Radiology, Arizona Health Sciences Center, University of Arizona,
Tucson, AZ 85724, U.S.A.*

and

*Optical Sciences Center, University of Arizona,
Tucson, AZ 85721, U.S.A.*

CONTENTS

§ 1. Introduction

The classic paper by RADON [1917] has had a far-reaching influence in many branches of science. What we now call the Radon transform arises in such diverse fields as X-ray crystallography, radio-astronomy, electron microscopy, diagnostic radiology, nuclear magnetic resonance, microwave scattering, and studies of the Fermi surface in metals. However, it is undoubtedly medical computed tomography (CT) that has attracted more attention than any other application of the Radon transform. The basic data obtained in a CT procedure are X-ray transmission measurements through a two-dimensional (2D) slice of the patient's body. Each measured transmission value is simply related to a line integral of the X-ray attenuation coefficient in this slice, and the set of all line integrals for a particular direction of the X-ray beam is a one-dimensional (1D) "projection" of the 2D object section. The set of all projections for all beam directions is the 2D Radon transform of the object, and reconstruction of the object from these projections is an implementation of the 2D inverse Radon transform.

Because of the overwhelming clinical and commercial success of CT, the 2D Radon transform has been studied in exhaustive detail. Its theoretical basis and practical limitations are very well understood. Much less attention has been given to the 3D Radon transform and its inverse, although many of the applications mentioned above are inherently three-dimensional.

The 3D Radon transform is a set of 1D functions obtained by integrating a 3D object over *planes*, as opposed to the line integrals that make up the 2D Radon transform. However, the structure of the inverse transform is different in the 2D and 3D cases, or, more generally, in spaces of odd and even dimensionality.

It is the purpose of this chapter to review our present state of knowledge about the Radon transform and to discuss some of its lesser-known applications. Although X-ray projections and tomographic reconstruction are used in § 2 as a starting point, this chapter is by no means a review of tomography. No consideration is given to such things as fan-beam geometries, iterative reconstruction algorithms, polyenergetic X-rays, detector noise, and clinical applica-

tions. These topics, which would be essential to any balanced treatment of tomography, are discussed in a number of books and review articles. See, for example, HERMAN [1980], BARRETT and SWINDELL [1981], KAK [1979], BROOKS and DiCHIRO [1976], GORDON, HERMAN and JOHNSON [1975], or SWINDELL and BARRETT [1977]. On the other hand, the chapter is also not a mathematical treatise in the rigorous theorem-proof sense. Rather, an attempt has been made to present the essential mathematical points in a way that is understandable to a scientist or engineer versed in Fourier theory, and to show that the Radon transform is a very useful tool in many practical applications. Those who require more rigor should consult the work of JOHN [1955], HELGASON [1965, 1980], LUDWIG [1966], SHEPP and KRUSKAL [1978], SMITH, SOLOMON and WAGNER [1977], GEL'FAND, GRAEV and VILENKIN [1966a,b] and DEANS [1978, 1983]. The conference proceedings edited by HERMAN and NATTERER [1981] and the recent treatise by DEANS [1983] contain a wealth of further mathematical references.

§ 2. The two-dimensional Radon transform

2.1. LINE INTEGRALS

It is usually a good approximation to assume that a thin pencil beam of monoenergetic X-rays is attenuated in accordance with Beer's law. For a homogeneous medium of thickness L, this means that

$$I = I_0 \, e^{-\mu L}, \tag{2.1}$$

where I is the X-ray flux transmitted through the medium, I_0 is the flux that would be transmitted in the absence of the medium, and μ is the linear attenuation coefficient. For an inhomogeneous medium such as the human body, $\mu = \mu(r)$ is a function of position, and (2.1) must be replaced with

$$I = I_0 \exp\left[-\int_S^D \mu(r) \, dl \right], \tag{2.2}$$

where the line integral runs from the source position S to the detector position D. In computed tomography, intensity measurements are made for many line-integral paths confined to a plane, and r is therefore a 2D position vector with Cartesian components (x, y).

The logarithm of I/I_0 is linearly related to the line integral:

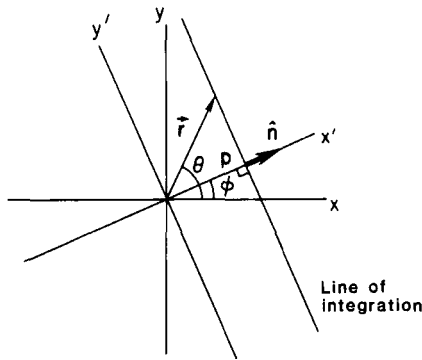$$-\ln(I/I_0) = \int_S^D \mu(r) \, dl. \tag{2.3}$$

Fig. 1. Geometry for the 2D Radon transform.

Therefore the measured transmissions directly yield values for the line integrals, and it is the goal of CT to reconstruct or estimate $\mu(r)$ from a finite set of its line integrals.

Two parameters are required to specify a line of integration (Fig. 1). For example, we can use the angle ϕ between the line and the y-axis and its perpendicular distance from the origin p, or we can use p and the unit normal to the line $\hat{n}$. We can then define the *projection* λ of a general 2D function $f(r)$ or $f(x, y)$ in several equivalent ways. If we choose a rotated coordinate system (x', y') such that the line of integration is parallel to the y'-axis, we can write

$$\lambda_\phi(p) \equiv \int_{-\infty}^{\infty} f_r(p, y') \, \mathrm{d}y', \tag{2.4}$$

where $f_r(x', y')$ denotes the same spatial distribution as $f(x, y)$, but expressed in the rotated system, i.e. $f_r(x', y') = f[x(x', y'), y(x', y')]$. Equation (2.4) defines the integral of f along the line $x' = p$.

An equivalent definition of $\lambda_\phi(p)$ is

$$\lambda_\phi(p) = \int_\infty \mathrm{d}^2r \, f(r)\delta(p - r \cdot \hat{n}), \tag{2.5}$$

where the subscript ∞ on the integral indicates that it runs over the infinite plane. The delta function in this equation is one-dimensional and has the effect of reducing the area integral to a line integral along the line $p = r \cdot \hat{n}$. The equivalence of (2.4) and (2.5) is easily demonstrated, since $f(r) = f_r(x', y')$,

$d^2r = dx' \, dy'$, and $x' = \boldsymbol{r} \cdot \hat{\boldsymbol{n}}$. Hence, (2.5) becomes

$$\lambda_\phi(p) = \int_{-\infty}^{\infty} dx' \int_{-\infty}^{\infty} dy' \, f_r(x', y') \delta(p - x')$$

$$= \int_{-\infty}^{\infty} dy' \, f_r(p, y'), \tag{2.6}$$

in agreement with (2.4).

It is sometimes convenient to define a vector

$$\boldsymbol{p} \equiv p\hat{\boldsymbol{n}} \tag{2.7}$$

and to write

$$\lambda_\phi(p) \equiv \lambda(\boldsymbol{p}). \tag{2.8}$$

We shall write $\lambda_\phi(p)$ when we wish to think of the projection as a 1D function with ϕ fixed, and $\lambda(\boldsymbol{p})$ when we wish to think of it as a 2D function. In the latter case, (2.5) may be regarded as an integral transform, the 2D Radon transform, connecting one 2D function, $f(\boldsymbol{r})$, to another, $\lambda(\boldsymbol{p})$. The space in which the vector $\boldsymbol{p}$ is defined is called *Radon space*, and a point in this space has polar coordinates (p, ϕ).

Note, however, that $\lambda(\boldsymbol{p})$ is not well behaved at the origin since $\lambda_{\phi_1}(0) \neq \lambda_{\phi_2}(0)$ (DEANS [1983]; LINDGREN and RATTEY [1981]).

Note also that $\lambda(\boldsymbol{p})$ and $f(\boldsymbol{r})$ share the same circular region of support (LUDWIG [1966]). More precisely, if $f(\boldsymbol{r}) = 0$ for $|\boldsymbol{r}| > R$, then $\lambda(\boldsymbol{p}) = 0$ for $|\boldsymbol{p}| > R$. This statement follows from (2.5) because the argument of the delta function does not vanish for any real $\hat{\boldsymbol{n}}$ if $|\boldsymbol{r}| < R$ and $|\boldsymbol{p}| > R$. More physically, if the line of integration does not pass through the region of support, the integral is zero.

Comparison of (2.6) with (2.3) shows that a single X-ray transmission measurement generates one point in the Radon transform of $\mu(\boldsymbol{r})$. (The limits of integration in (2.3) may be extended to $\pm \infty$ if $\mu(\boldsymbol{r})$ is zero outside a finite region.) In practice, only a finite set of transmission measurements is made, and each measurement suffers some inaccuracy, at the very least that due to shot noise in the X-ray beam. It is therefore impossible to determine $\mu(\boldsymbol{r})$ uniquely, and practical CT reconstruction algorithms seek the "best" estimate of $\mu(\boldsymbol{r})$. These algorithms are discussed fully by HERMAN [1980] and BARRETT and SWINDELL [1981], but they are not the concern of this chapter. Instead, we shall assume that $\lambda(\boldsymbol{p})$ is known exactly for all points in Radon space (i.e., all values of p and ϕ). We seek, therefore, the mathematically exact form of the

2D inverse Radon transform that will enable us to find $f(\mathbf{r})$ given $\lambda(p)$. For a detailed discussion of the *discrete* Radon transform, when only a finite set of line integrals is known, see LINDGREN and RATTEY [1981].

2.2. THE CENTRAL-SLICE THEOREM

What information about $f(\mathbf{r})$ is contained in each 1D projection $\lambda_\phi(p)$? To answer this question, we take the 1D Fourier transform of $\lambda_\phi(p)$:

$$\Lambda_\phi(\nu) = \mathscr{F}_1\{\lambda_\phi(p)\} = \int_{-\infty}^{\infty} dp\, \lambda_\phi(p) \exp(-2\pi i \nu p), \qquad (2.9)$$

where $\mathscr{F}_m$ is the m-dimensional Fourier operator and ν is the frequency variable conjugate to p. Using (2.4) and changing the variable of integration from p to x', we find

$$\Lambda_\phi(\nu) = \int_{-\infty}^{\infty} dx' \int_{-\infty}^{\infty} dy'\, f_r(x', y') \exp(-2\pi i \nu x'). \qquad (2.10)$$

This result is to be compared to the general definition of the 2D Fourier transform:

$$F(\boldsymbol{\rho}) = \mathscr{F}_2\{f(\mathbf{r})\} = \int_{\infty} d^2r\, f(\mathbf{r}) \exp(-2\pi i \boldsymbol{\rho} \cdot \mathbf{r})$$

$$= \int_{-\infty}^{\infty} dx \int_{-\infty}^{\infty} dy\, f(x, y) \exp[-2\pi i(\xi x + \eta y)], \quad (2.11)$$

where $\boldsymbol{\rho}$ is a 2D spatial-frequency vector with Cartesian components ξ and η. We shall consistently use capital letters to denote the Fourier transform of the corresponding lower-case function. Comparing (2.11) and (2.10), we see that

$$\Lambda_\phi(\nu) = F_r(\xi', \eta')\Big|_{\substack{\xi' = \nu \\ \eta' = 0}} = F_r(\nu, 0), \qquad (2.12)$$

where ξ' and η' are the frequency components in a rotated system (Fig. 2) and are therefore conjugate to x' and y', respectively. This important result, known as the central-slice or projection-slice theorem, shows that *the 1D Fourier transform of a projection of a 2D function is directly one line through the 2D Fourier transform of the function itself*. The line is the ξ' axis in the rotated frequency-space coordinates. The entire 2D frequency space can thus be sampled on a set of lines passing through the origin (hence the word "central") by transforming projections at different angles ϕ.
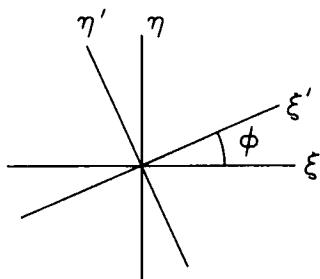
Fig. 2. Geometry of 2D Fourier space, showing rotated coordinates.

An alternative derivation of the central-slice theorem without rotated coordinates proceeds from (2.5). A 1D Fourier transform of this equation yields

$$\Lambda_\phi(v) = \int_{-\infty}^{\infty} dp \exp(-2\pi i v p) \int_\infty d^2r\, f(r)\delta(p - r \cdot \hat{n})$$

$$= \int_\infty d^2r\, f(r) \exp(-2\pi i r \cdot \hat{n} v)$$

$$= F(\rho)|_{\rho = \hat{n}v} = F(\hat{n}v). \tag{2.13}$$

The condition $\rho = \hat{n}v$ is the same as $\xi' = v$ since the ξ' axis is parallel to $\hat{n}$, and thus (2.13) is equivalent to (2.12).

With this theorem, we can now more precisely define a "complete" projection data set. The transform $F(\rho)$ can be determined for all ρ, and hence $f(r)$ is uniquely determined, if $\lambda_\phi(p)$ is known for $-\infty < p < \infty$ and $0 < \phi \le \pi$. It is not necessary for the range in ϕ to exceed π because of the symmetry relation,

$$\lambda_\phi(p) = \lambda_{\phi + \pi}(-p), \tag{2.14}$$

which is easily derived from (2.5) by noting that $\delta(x) = \delta(-x)$ and that the change $\phi \to \phi + \pi$ implies $\hat{n} \to -\hat{n}$. Equation (2.14) also follows from the truism $p = p\hat{n} = (-p)(-\hat{n})$. Hence, polar coordinates (p, ϕ) and $(-p, \phi + \pi)$ denote the same point p in Radon space. Because of (2.14), the projection data set is also complete if $\lambda_\phi(p)$ is known for $0 \le p < \infty$ and $0 < \phi \le 2\pi$. In practice, the projection data are usually sampled in both p and ϕ, but we shall treat both as continuous variables.

2.3. THE INVERSE 2D RADON TRANSFORM

The quickest route to the inverse Radon transform is via the central-slice theorem. We need only take the inverse Fourier transform of (2.13), expressing ρ in polar coordinates (ρ, θ_ρ). However, it will simplify the algebra somewhat if we allow ρ to take on positive and negative values and restrict θ_ρ to $(0, \pi)$. Then the form of the 2D inverse Fourier transform is

$$f(\mathbf{r}) = \int_{-\infty}^{\infty} |\rho| \, d\rho \int_0^\pi d\theta_\rho \, F(\boldsymbol{\rho}) \exp(2\pi i \boldsymbol{\rho} \cdot \mathbf{r}). \qquad (2.15)$$

We now let $\boldsymbol{\rho} = \hat{\mathbf{n}} v$, which implies that $\rho = v$ and $\theta_\rho = \phi$, and use (2.13), yielding

$$f(\mathbf{r}) = \int_{-\infty}^{\infty} |v| \, dv \int_0^\pi d\phi \, \Lambda_\phi(v) \exp(2\pi i v \mathbf{r} \cdot \hat{\mathbf{n}}). \qquad (2.16)$$

This is one form of the 2D inverse Radon transform since (2.16), along with (2.9), allows us to determine $f(\mathbf{r})$ from $\lambda_\phi(p)$.

A more familiar form of the inverse Radon transform is obtained by rewriting (2.16) as

$$f(\mathbf{r}) = \int_0^\pi d\phi \left[\int_{-\infty}^{\infty} K_\phi(v) e^{2\pi i v p} \, dv \right]_{p = \mathbf{r} \cdot \hat{\mathbf{n}}}, \qquad (2.17)$$

where

$$K_\phi(v) \equiv |v| \Lambda_\phi(v). \qquad (2.18)$$

The v-integral in (2.17) is an inverse 1D Fourier transform, and, by the convolution theorem (GASKILL [1978]), we have

$$f(\mathbf{r}) = \int_0^\pi d\phi \left[\lambda_\phi(p) * \mathscr{F}_1^{-1}\{|v|\} \right]_{p = \mathbf{r} \cdot \hat{\mathbf{n}}}, \qquad (2.19)$$

with the asterisk denoting 1D convolution and $\mathscr{F}_m^{-1}$ being the inverse m-dimensional Fourier operator. From LIGHTHILL [1962],

$$\mathscr{F}_1^{-1}\{|v|\} = \frac{-1}{2\pi^2 p^2}, \qquad (2.20)$$

and (2.19) therefore becomes

$$f(\mathbf{r}) = -\frac{1}{2\pi^2} \int_0^\pi d\phi \left[\lambda_\phi(p) * \frac{1}{p^2} \right]_{p = \mathbf{r} \cdot \hat{\mathbf{n}}}, \qquad (2.21)$$

which is an often-quoted form of the 2D inverse Radon transform.

The function $1/p^2$ in (2.20) and (2.21) must be interpreted as a generalized function. To see that it cannot be taken at face value, suppose that $f(r)$ is everywhere nonnegative. Then the projection $\lambda_\phi(p)$ must also be nonnegative and, if we interpret $1/p^2$ blindly as a positive number, the integral in (2.21) is nonnegative. However, there is an overall minus sign in front of the integral, and (2.21) predicts that $f(r)$ is negative, in contradiction to our original assumption.

One approach to the interpretation of $1/p^2$ is by use of the central-ordinate theorem of Fourier theory (GASKILL [1978]). We let $H(v) = |v|$ and denote the inverse Fourier transform of $H(v)$ by $h(p)$. Then

$$\int_{-\infty}^{\infty} h(p)\,\mathrm{d}p = H(0) = 0. \tag{2.22}$$

Hence, $h(p)$ cannot be everywhere negative, and (2.20) cannot be correct for all p. If we accept (2.20) for $p \neq 0$, we might be tempted to add a delta function $C\delta(p)$ to (2.20) and adjust C to satisfy (2.22). Then we could write

$$\int_{-\infty}^{\infty} h(p)\,\mathrm{d}p = \lim_{\varepsilon \to 0}\left[\int_{-\infty}^{-\varepsilon}\mathrm{d}p + \int_{\varepsilon}^{\infty}\mathrm{d}p\right]\left(\frac{-1}{2\pi^2 p^2}\right) + \lim_{\varepsilon \to 0}\int_{-\varepsilon}^{\varepsilon} C\delta(p)$$

$$= \lim_{\varepsilon \to 0}\left[-\frac{1}{\pi^2 \varepsilon} + C\right] = 0. \tag{2.23}$$

For this patch to work, we must let $C \to \infty$ as $\varepsilon \to 0$, which says that the generalized function $1/p^2$ behaves as a negative delta function of infinite weight at $p = 0$.

Another approach to the interpretation of this function is to write

$$|v| = v \operatorname{sgn} v = 2\pi i v \frac{\operatorname{sgn} v}{2\pi i}, \tag{2.24}$$

where

$$\operatorname{sgn} v \equiv \begin{cases} +1 & v > 0 \\ 0 & v = 0 \\ -1 & v < 0. \end{cases} \tag{2.25}$$

It is known (BRACEWELL [1965], GASKILL [1978]) that

$$\mathscr{F}_1^{-1}\{2\pi i v\} = \delta'(p) \tag{2.26}$$

and

$$\mathscr{F}_1^{-1}\left\{\frac{\operatorname{sgn} v}{2\pi i}\right\} = \frac{1}{2\pi^2}\,\mathscr{P}\left(\frac{1}{p}\right), \tag{2.27}$$

where $\delta'(p)$ is the first derivative of a 1D delta function and $\mathscr{P}$ denotes a Cauchy principal value. From these equations and the convolution theorem, we have

$$h(p) = \delta'(p) * \left(\frac{1}{2\pi^2}\right) \mathscr{P}\left(\frac{1}{p}\right), \tag{2.28}$$

Then we can rewrite (2.19) as

$$f(\mathbf{r}) = \frac{1}{2\pi^2} \mathscr{P} \int_0^\pi d\phi \left[\lambda_\phi(p) * \delta'(p) * \frac{1}{p}\right]_{p = \mathbf{r} \cdot \hat{n}}$$

$$= \frac{1}{2\pi^2} \mathscr{P} \int_0^\pi d\phi \left[\lambda'_\phi(p) * \frac{1}{p}\right]_{p = \mathbf{r} \cdot \hat{n}}, \tag{2.29}$$

where $\lambda'_\phi(p) \equiv \partial \lambda_\phi(p)/\partial p$, and the last step in (2.29) follows from the definition of $\delta'(p)$. Note that $\mathscr{P}$ refers to the convolution, not the integral over ϕ.

Since convolution with $(-1/\pi)\mathscr{P}(1/p)$ is equivalent to Hilbert transformation (BRACEWELL [1965]), the quantity in brackets in (2.29) is proportional to the Hilbert transform of the derivative of the projection data.

An integration by parts leads from (2.29) back to (2.21) if we interpret $1/p^2$ by

$$\frac{1}{p^2} = -\frac{d}{dp} \mathscr{P}\left(\frac{1}{p}\right). \tag{2.30}$$

The origin of the infinite-weight delta now becomes clearer; it represents the derivative of the infinite discontinuity of $\mathscr{P}(1/p)$ at $p = 0$.

Another form of the inverse Radon transform is obtained by writing

$$\frac{d}{dp} \ln|p| = \mathscr{P}\left(\frac{1}{p}\right), \tag{2.31}$$

which is clearly correct for $p \neq 0$, and may be regarded as a definition for $p = 0$ (LIGHTHILL [1962]). An integration by parts in (2.29) then yields

$$f(\mathbf{r}) = \frac{1}{2\pi^2} \int_0^\pi d\phi [\lambda''_\phi(p) * \ln|p|]_{p = \mathbf{r} \cdot \hat{n}}, \tag{2.32}$$

where $\lambda''_\phi(p) = \partial^2 \lambda_\phi(p)/\partial p^2$. It can also be shown that

$$\frac{d^2 f(x)}{dx^2} * g(x) = f(x) * \frac{d^2 g(x)}{dx^2} = \frac{d^2}{dx^2} [f(x) * g(x)], \tag{2.33}$$

where $f(x)$ and $g(x)$ are arbitrary differentiable functions. The proof of this equation follows by Fourier-transforming both sides. Using (2.33), we can rewrite (2.32) as

$$f(\mathbf{r}) = \frac{1}{2\pi^2} \int_0^\pi d\phi \left\{ \frac{\partial^2}{\partial p^2} [\lambda_\phi(p) * \ln|p|] \right\}_{p = \mathbf{r} \cdot \hat{n}}. \tag{2.34}$$

Still another version of the inverse Radon transform is

$$f(\mathbf{r}) = \frac{1}{2\pi^2} \nabla^2 \int_0^\pi d\phi [\lambda_\phi(p) * \ln|p|]_{p = \mathbf{r} \cdot \hat{n}}. \tag{2.35}$$

Equation (2.35) follows from (2.34) and the general result,

$$\nabla^2 g(\mathbf{r} \cdot \hat{n}) = \frac{d^2 g(p)}{dp^2} \bigg|_{p = \mathbf{r} \cdot \hat{n}} = g''(\mathbf{r} \cdot \hat{n}), \tag{2.36}$$

which is easily proven by using a Cartesian coordinate system with $\hat{n}$ parallel to one of the axes. Equation (2.36) is valid in any number of dimensions and will prove useful in discussing the 3D Radon transform. (COURANT and HILBERT [1962], p. 681.)

2.4. BACK-PROJECTION AND SUMMATION

In all of the forms of the inverse Radon transform given in the last section, the substitution $p = \mathbf{r} \cdot \hat{n}$ appeared. This operation has a simple physical interpretation; it converts a 1D function $g(p)$ into a 2D function $g(\mathbf{r} \cdot \hat{n})$ that shows no variation in the direction perpendicular to $\hat{n}$. That is, $g(p)$ is smeared or *back-projected* along the original projection direction, which is the y'-axis in Fig. 1. All points in the $\mathbf{r}$-plane with the same x'-coordinate are assigned the same value $g(x')$, since $x' = \mathbf{r} \cdot \hat{n}$.

The *summation image* $b(\mathbf{r})$ results when all projections $\lambda_\phi(p)$ are back-projected and the resulting 2D image is summed over all projection angles ϕ. Since we are treating the data set as continuous, the sum becomes an integral and we have

$$b(\mathbf{r}) \equiv \int_0^\pi d\phi \, \lambda_\phi(\mathbf{r} \cdot \hat{n}). \tag{2.37}$$

An illustration of a summation image is given in Fig. 3. It is almost always a poor representation of $f(\mathbf{r})$.
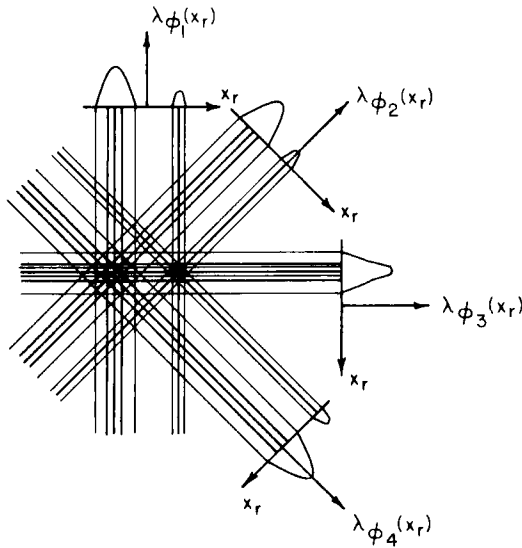
Fig. 3. Illustration of a summation image, from BARRETT and SWINDELL [1981]. The original object was two discs, and only four projections are shown. The rotated coordinate x_r corresponds to p in the text.

To see the relationship between $f(r)$ and $b(r)$, it is convenient to consider a point object,

$$f^\delta(r) \equiv \delta(r - r_0), \tag{2.38}$$

where $\delta(r - r_0)$ is a 2D delta function. By (2.5), the projections of this object are

$$\lambda_\phi(p) = \int_\infty d^2r \, \delta(r - r_0)\delta(p - r \cdot \hat{n}) = \delta(p - r_0 \cdot \hat{n}). \tag{2.39}$$

Thus each projection of a 2D delta function is a 1D delta function. (Note that we distinguish 1D and 2D delta functions only by their arguments; if the argument is a scalar, the delta function is 1D, and if the argument is an mD vector, the delta function is mD.) Using (2.39) in (2.37), we see that the summation image is given by

$$b^\delta(r) = \int_0^\pi d\phi \, \delta[(r - r_0) \cdot \hat{n}], \tag{2.40}$$

where the superscript δ is a reminder that we are dealing with a particular point object.

To perform the integral in (2.40), we denote the angle between $r - r_0$ and the x-axis by ψ and write

$$b^\delta(r) = \int_0^\pi d\phi \, \delta[\,|r - r_0| \cos(\psi - \phi)]. \tag{2.41}$$

The argument of the delta function is zero exactly once in the range $0 < \phi \leq \pi$, namely when $\phi = \phi_0$, where ϕ_0 is either $\psi \pm \pi/2$ or $\psi \pm 3\pi/2$, whichever falls in $(0, \pi)$. In the neighborhood of ϕ_0, $\cos(\psi - \phi) = \pm(\phi - \phi_0)$, and we have

$$b^\delta(r) = \int_0^\pi d\phi \, \delta[\,\pm |r - r_0|(\phi - \phi_0)] = \frac{1}{|r - r_0|}, \tag{2.42}$$

since $\delta(\alpha x) = \delta(x)/|\alpha|$ for α constant.

Thus, for a point object, the summation image has the cusp-like form $|r - r_0|^{-1}$. The point spread function for back-projection and summation is $|r|^{-1}$, and the summation image for a more general object is

$$b(r) = \int_\infty d^2 r_0 \, f(r_0) \frac{1}{|r - r_0|} = f(r) ** \frac{1}{|r|}, \tag{2.43}$$

where the double asterisk denotes 2D convolution.

The blur function $1/|r|$ can be removed by suitably filtering $b(r)$. Since $1/|r|$ is rotationally symmetric, its 2D Fourier transform becomes a Hankel transform (GASKILL [1978]) given by

$$\mathscr{F}_2\left\{\frac{1}{|r|}\right\} = 2\pi \int_0^\infty r \, dr \cdot \frac{1}{r} J_0(2\pi\rho r) = \frac{1}{|\rho|} \int_0^\infty J_0(u) \, du = \frac{1}{|\rho|}, \tag{2.44}$$

where $u = 2\pi\rho r$ and $J_0(u)$ is the zero-order Bessel function of the first kind. Thus the frequency-domain counterpart of (2.43) is

$$B(\rho) = F(\rho) \cdot \frac{1}{|\rho|}. \tag{2.45}$$

Multiplication of (2.45) by $|\rho|$ and inverse Fourier transformation yields

$$f(r) = \mathscr{F}_2^{-1}\{|\rho| B(\rho)\}. \tag{2.46}$$

This result, along with the definition (2.37) of $b(r)$, constitutes yet another form of the 2D inverse Radon transform.

It is interesting to compare (2.46) to (2.16). The steps involved in going from $\lambda_\phi(p)$ to $f(r)$ by use of (2.16) are:
1. Fourier transform (1D);
2. filter (1D) with transfer function $|\nu|$;
3. inverse Fourier transform (1D);
4. back-project (1D → 2D);
5. integrate over ϕ.

The corresponding steps with (2.46) and (2.37) are:
1. back-project (1D → 2D);
2. integrate over ϕ;
3. Fourier transform (2D);
4. filter (2D) with transfer function $|\rho|$;
5. inverse Fourier transform (2D).

Note that all of the same steps are involved, but in a different order. In the first case, the filtering occurs before back-projection and is therefore 1D, while in the second case it is after back-projection and therefore 2D. It is the central-slice theorem that guarantees the equivalence of 1D and 2D filtering. In both cases, of course, the filtering could also be carried out in the space domain.

In practice, neither the 1D nor the 2D filter can have the ideal form, $|\nu|$ or $|\rho|$, since that would imply an infinite boost as the frequency goes to infinity. Instead, the filter must be rolled off at high frequencies or *apodized* by some function $A(\nu)$ or $A(\rho)$. The resulting counterparts of eqs. (2.16) and (2.46) are no longer mathematically exact inverse transforms, but they perform better with real, noisy input data since they do not attempt an infinite boost. The literature on apodizing functions is, however, rapidly approaching infinity, and we shall not add to it here.

2.5. SUMMARY IN OPERATOR FORM

The 2D Radon transform may be written in shorthand as

$$\lambda = \mathscr{R}_2\{f\}, \tag{2.47}$$

where λ represents the set of functions $\lambda_\phi(p)$ for all ϕ and p, f represents $f(r)$ for all r, and $\mathscr{R}_2$ is the integral operator defined by (2.4) or (2.5). All of the equivalent forms of the inverse Radon transform are then implementations of the operator $\mathscr{R}_2^{-1}$, where

$$f = \mathscr{R}_2^{-1}\{\lambda\}. \tag{2.48}$$

We have already introduced the 1D and 2D Fourier-transform operators, in terms of which (cf. (2.10) and (2.11)),

$$\Lambda = \mathscr{F}_1\{\lambda\}; \qquad F = \mathscr{F}_2\{f\}. \tag{2.49}$$

With these operators, the central slice theorem (2.12) or (2.13) reads

$$\mathscr{F}_2\{f\} = \mathscr{F}_1\mathscr{R}_2\{f\}, \tag{2.50a}$$

or, as a pure operator relation,

$$\mathscr{F}_2 = \mathscr{F}_1\mathscr{R}_2. \tag{2.50b}$$

By the usual rules for operator manipulation, (2.50b) becomes

$$\mathscr{R}_2^{-1} = \mathscr{F}_2^{-1}\mathscr{F}_1, \tag{2.51}$$

which is just (2.16).

To express the other equivalent forms of $\mathscr{R}_2^{-1}$, we must define two more operators. The 2D back-projection and summation operator $\mathscr{B}_2$ involves the substitution $p = \mathbf{r}\cdot\hat{\mathbf{n}}$, which is back-projection itself, and integration over ϕ ("summation"). Thus (2.37) may be written

$$b = \mathscr{B}_2\{\lambda\}, \tag{2.52}$$

where $b = b(\mathbf{r})$. Mathematically, $\mathscr{B}_2$ is the adjoint of $\mathscr{R}_2$ (LUDWIG [1966]).

The other operator we need is the Hilbert-transform operator $\mathscr{H}$, given by (BRACEWELL [1965])

$$\mathscr{H} = \frac{-1}{\pi p} *, \tag{2.53}$$

where the Cauchy principal value of $1/p$ is understood, and the asterisk still denotes 1D convolution.

Equations (2.17) and (2.21) may now be written

$$\mathscr{R}_2^{-1} = \mathscr{B}_2\mathscr{F}_1^{-1}|\nu|\mathscr{F}_1 = -\frac{1}{2\pi^2}\mathscr{B}_2\left[\frac{1}{p^2} *\right], \tag{2.54}$$

depending on whether the 1D convolution is to be carried out in the p-domain or the ν-domain. When applied to λ, (2.54) shows that the 1D projections must each be convolved with the generalized function $1/p^2$, then back-projected and summed in order to reconstruct f.

Equation (2.29) becomes

$$\mathscr{R}_2^{-1} = \frac{1}{2\pi^2} \mathscr{B}_2 \left[\frac{1}{p} * \right] \frac{\partial}{\partial p} = -\frac{1}{2\pi} \mathscr{B}_2 \mathscr{H} \frac{\partial}{\partial p}, \qquad (2.55)$$

while (2.32) and (2.35) become

$$\mathscr{R}_2^{-1} = \frac{1}{2\pi^2} \mathscr{B}_2 [\ln |p| *] \frac{\partial^2}{\partial p^2} = \frac{1}{2\pi^2} \nabla^2 \mathscr{B}_2 [\ln |p| *]. \qquad (2.56)$$

To show the consistency of these relations, let us retrace the route from (2.56) to (2.54) with operators. The only additional information needed is the 1D Fourier transform of $\ln |p|$ (LIGHTHILL [1962]):

$$\mathscr{F}_1 \{ \ln |p| \} = \frac{-1}{2|v|}, \qquad (2.57)$$

or, in operator form

$$\mathscr{F}_1 [\ln |p| *] = \frac{-1}{2|v|} \mathscr{F}_1. \qquad (2.58)$$

Note that the square brackets around $[\ln |p| *]$ indicate that it is an *operator*, while the curly brackets in (2.57) indicate that $\ln |p|$ is the *operand* of $\mathscr{F}_1$. The equivalence of (2.57) and (2.58) follows from the usual Fourier convolution theorem (GASKILL [1978]), and may easily be seen by operating on $\delta(p)$ with (2.58).

The Fourier derivative theorem (GASKILL, 1978) in operator form is

$$\mathscr{F}_1 \frac{\partial^n}{\partial p^n} = (2\pi i v)^n \mathscr{F}_1. \qquad (2.59)$$

Using (2.58) and (2.59) in the first form of (2.56), we find

$$\mathscr{R}_2^{-1} = \frac{1}{2\pi^2} \mathscr{B}_2 [\ln |p| *] \frac{\partial^2}{\partial p^2}$$

$$= \frac{1}{2\pi^2} \mathscr{B}_2 \mathscr{F}_1^{-1} \left[\frac{-1}{2|v|} \right] \mathscr{F}_1 \mathscr{F}_1^{-1} [-4\pi^2 v^2] \mathscr{F}_1$$

$$= \frac{1}{2\pi^2} \mathscr{B}_2 \mathscr{F}_1^{-1} [2\pi^2 |v|] \mathscr{F}_1, \qquad (2.60)$$

which is just (2.54).

§ 3. The Three-Dimensional Radon Transform

3.1. PLANAR INTEGRALS

Three independent parameters are required to specify a plane in a 3D space. For example, we can use the unit normal $\hat{n}$ and the distance from the origin p as shown in Fig. 4. The three parameters in this case are p and the polar angles θ_n and ϕ_n that specify $\hat{n}$ (Fig. 4b), and the equation of the plane is $p = r \cdot \hat{n}$, where sans-serif type indicates 3D quantities, and $r = (x, y, z)$ is the general 3D position vector. In a rotated coordinate system (x', y', z') such that x' is normal to the plane, the equation of the plane is $p = x'$.

An integral of a 3D function $f(r)$ or $f(x, y, z)$ over this plane is given by

$$\lambda_{\hat{n}}(p) = \int_{-\infty}^{\infty} dy' \int_{-\infty}^{\infty} dz' \, f_r(p, y', z') = \int_{\infty} d^3r \, f(r) \delta(p - r \cdot \hat{n}), \quad (3.1)$$

where $f_r(x', y', z')$ is the same physical distribution as $f(x, y, z)$, but expressed in the rotated coordinates.

As in the 2D case, it is sometimes convenient to define a 3D Radon space, with

$$p = p\hat{n} \quad (3.2)$$

specifying a point in that space. The spherical polar components of the vector p are (p, θ_n, ϕ_n). We shall write $\lambda(p)$ when we wish to regard λ as a 3D function and $\lambda_{\hat{n}}(p)$ when we wish to regard it as a set of 1D functions. In either case,
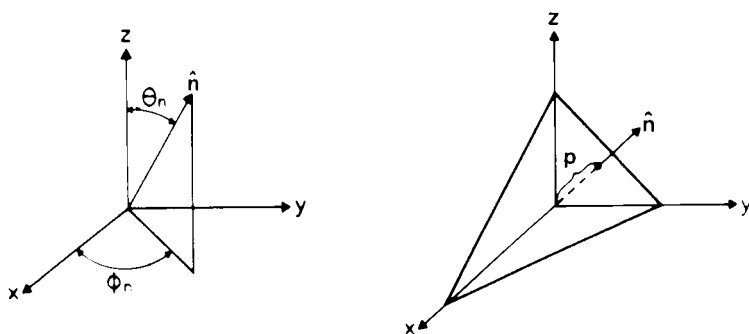

Fig. 4. (a) Geometry for the 3D Radon transform, showing a plane of integration with unit normal $\hat{n}$ and perpendicular distance from the origin p. (b) The vector $\hat{n}$ is specified by polar coordinates θ_n and ϕ_n.

(3.1) defines the 3D Radon transform, and we can write it symbolically as

$$\lambda = \mathscr{R}_3\{f\}, \tag{3.3}$$

where $\mathscr{R}_3$ is the 3D Radon operator.

Note that, as in the 2D case, $\lambda(\boldsymbol{p})$ and $f(\boldsymbol{r})$ share the same spherical region of support. If $f(\boldsymbol{r}) = 0$ for $|\boldsymbol{r}| > R$, then $\lambda(\boldsymbol{p}) = 0$ for $|\boldsymbol{p}| > R$.

3.2. THE CENTRAL-SLICE THEOREM

The derivation of the 3D central-slice theorem exactly follows the 2D derivation in § 2.2. A 1D Fourier transform of the first form of (3.1) is

$$\Lambda_{\hat{n}}(v) = \int_{-\infty}^{\infty} \mathrm{d}p\, \lambda_{\hat{n}}(p) \exp(-2\pi i v p). \tag{3.4}$$

Letting $p = x'$ and using (3.1), we get

$$\Lambda_{\hat{n}}(v) = \int_{-\infty}^{\infty} \mathrm{d}x' \int_{-\infty}^{\infty} \mathrm{d}y' \int_{-\infty}^{\infty} \mathrm{d}z'\, f_{\mathrm{r}}(x', y', z') \exp(-2\pi i v x')$$

$$= F_{\mathrm{r}}(v, 0, 0), \tag{3.5}$$

where $F_{\mathrm{r}}(\xi', \eta', \zeta')$ is the 3D Fourier transform of $f_{\mathrm{r}}(x', y', z')$. In general, the 3D Fourier transform is defined by

$$F(\boldsymbol{\sigma}) = F(\xi, \eta, \zeta) = \int_{\infty} \mathrm{d}^3 r\, f(\boldsymbol{r}) \exp(-2\pi i \boldsymbol{\sigma} \cdot \boldsymbol{r}). \tag{3.6}$$

Equation (3.5) is the 3D central-slice theorem in rotated coordinates, the 3D counterpart of (2.12).

An alternative expression of this theorem without rotated coordinates is found from a 1D Fourier transformation of the second form of (3.1):

$$\Lambda_{\hat{n}}(v) = \int_{-\infty}^{\infty} \mathrm{d}p \exp(-2\pi i p v) \int_{\infty} \mathrm{d}^3 r\, f(\boldsymbol{r}) \delta(p - \boldsymbol{r} \cdot \hat{n})$$

$$= \int_{\infty} \mathrm{d}^3 r\, f(\boldsymbol{r}) \exp(-2\pi i \boldsymbol{r} \cdot \hat{n} v)$$

$$= F(\hat{n} v). \tag{3.7}$$

Both (3.6) and (3.7) show that *the 1D Fourier transform of a planar projection of a 3D function is one line through the 3D Fourier transform of the function itself.*

The orientation of this line in 3D Fourier space is determined by $\hat{n}$, the normal to the original plane of integration.

If $\hat{n}$ explores all directions in a hemisphere and p ranges from $-\infty$ to ∞, enough information is obtained to determine $F(\sigma)$ and hence $f(r)$. Of course, physically meaningful functions have bounded support, so only a finite range in p is needed in practice. If measurements are made only for positive p, then $\hat{n}$ must explore a full sphere of directions to completely determine $F(\sigma)$.

3.3. THE INVERSE 3D RADON TRANSFORM

As in the 2D case, the shortest route to the inverse 3D Radon transform is via the central-slice theorem. We must take a 3D inverse Fourier transform of (3.7) in polar coordinates, where σ has components $(\sigma, \theta_\sigma, \phi_\sigma)$. We allow σ to take on positive and negative values and restrict the direction of σ to a hemisphere. Then the form of the 3D inverse Fourier transform is

$$f(r) = \int_{-\infty}^{\infty} \sigma^2 \, d\sigma \int_{2\pi} d\Omega_\sigma \, F(\sigma) \exp(2\pi i \sigma \cdot r), \qquad (3.8)$$

where $d\Omega_\sigma = \sin \theta_\sigma \, d\theta_\sigma \, d\phi_\sigma$, and the angular integral extends over 2π ster. In order to use (3.7), we let $\sigma = \hat{n} v$, which implies that $\sigma = v$, $\theta_n = \theta_\sigma$, $\phi_n = \phi_\sigma$. Then (3.8) becomes [cf. (2.16)]:

$$f(r) = \int_{-\infty}^{\infty} v^2 \, dv \int_{2\pi} d\Omega_n \, \Lambda_{\hat{n}}(v) \exp(2\pi i v r \cdot \hat{n}), \qquad (3.9)$$

which is one form of the 3D inverse Radon transform.

An equivalent form is obtained by rewriting (3.9) as

$$f(r) = \int_{2\pi} d\Omega_n \, \mathscr{F}_1^{-1} \{ v^2 \Lambda_{\hat{n}}(v) \}_{p = r \cdot \hat{n}}$$

$$= -\frac{1}{4\pi^2} \int_{2\pi} d\Omega_n [\lambda_{\hat{n}}''(p)]_{p = r \cdot \hat{n}}$$

$$= -\frac{1}{4\pi^2} \int_{2\pi} d\Omega_n \, \lambda_{\hat{n}}''(r \cdot \hat{n}), \qquad (3.10)$$

where $\lambda_{\hat{n}}''(p) = \partial^2 \lambda_{\hat{n}}(p)/\partial p^2$, and the 1D Fourier derivative theorem (2.59) has been used.

Another form of the inverse transform follows at once from (3.10) and (2.36):

$$f(r) = -\frac{1}{4\pi^2} \nabla^2 \int_{2\pi} d\Omega_n \, \lambda_n(r \cdot \hat{n}). \tag{3.11}$$

Note that (3.10) and (3.11) are somewhat simpler than their 2D counterparts, (2.32) and (2.35), since the convolution with $\ln|p|$ is not required in 3D.

3.4. BACK-PROJECTION AND SUMMATION

The substitution $p = r \cdot \hat{n}$ in (3.10) and (3.11) is 3D-back-projection. It assigns the same value to all points on the plane $p = r \cdot \hat{n}$, which is the original plane of integration. When each 1D projection $\lambda_n(p)$ is back-projected and the resulting 3D function is summed (integrated) over all directions of $\hat{n}$, the result is the 3D summation image $b(r)$, defined by [cf. (2.37)]

$$b(r) \equiv \int_{2\pi} d\Omega_n \, \lambda_n(r \cdot \hat{n}). \tag{3.12}$$

Of course, $b(r)$ is not an accurate image of $f(r)$. To find the relationship between $b(r)$ and $f(r)$, we again consider a point object as in § 2.4:

$$f^\delta(r) = \delta(r - r_0). \tag{3.13}$$

By arguments similar to those of (2.38)–(2.42), we can show (CHIU [1980]) that the projection of this 3D delta function is the 1D delta function,

$$\lambda_n(p) = \delta(p - r_0 \cdot \hat{n}), \tag{3.14}$$

and that the corresponding summation image is

$$b^\delta(r) = \frac{\pi}{|r - r_0|}. \tag{3.15}$$

Thus, the point spread function in the summation image has the same functional form as in the 2D case [cf. (2.42)], and the summation image for a more general object is [cf. (2.43)]

$$b(r) = \pi \int_\infty d^3 r_0 \, f(r_0) \frac{1}{|r - r_0|}$$

$$= \pi f(r) * * * \frac{1}{|r|}, \tag{3.16}$$

where the triple asterisk denotes 3D convolution.

One way of recovering $f(r)$ from $b(r)$ is by 3D frequency-domain filtering. The 3D Fourier transform of (3.16) is

$$\mathcal{B}(\sigma) = \pi F(\sigma) \mathcal{F}_3 \left\{ \frac{1}{|r|} \right\}. \tag{3.17}$$

From CHIU [1980],

$$\mathcal{F}_3 \left\{ \frac{1}{|r|} \right\} = \frac{1}{\pi \sigma^2}, \tag{3.18}$$

so that the required filter transfer function is proportional to σ^2, and

$$f(r) = \mathcal{F}_3^{-1} \{ F(\sigma) \} = \mathcal{F}_3^{-1} \{ \sigma^2 \mathcal{B}(\sigma) \}. \tag{3.19}$$

Note, however, that multiplication by $-4\pi^2\sigma^2$ in the 3D frequency domain is the same as taking the Laplacian in the space domain. Therefore,

$$f(r) = -\frac{1}{4\pi^2} \nabla^2 b(r), \tag{3.20}$$

which, with (3.12), is the result previously derived in (3.11). Still another route to the same result is by applying the operator ∇^2 to (3.16), taking it under the integral sign, and recognizing that

$$\nabla^2 \frac{1}{|r - r_0|} = -4\pi\delta(r - r_0), \tag{3.21}$$

which is simply Poisson's equation for a point charge. The delta function in (3.21) is then used to perform the integral in (3.16), again yielding (3.20). The Laplacian therefore undoes the $1/|r|$ blurring brought about by back-projection and summation.

It is interesting to note that the filtering operations required in the 3D Radon transform are *local*; they are simple second derivatives; ∇^2 or $\partial^2/\partial p^2$, that can be computed using only values of the function in the immediate neighborhood of the point at which the derivative is evaluated. By contrast, the 2D inverse transform requires convolution with either $1/p^2$, $1/p$, or $\ln|p|$, all of which have tails extending to $\pm\infty$. Basically, the local character of the 3D space-domain filter comes from the smoothness of the frequency-domain filter σ^2 or v^2, while the slope discontinuity in the 2D filter, $|\rho|$ or $|v|$, causes the tails in the 2D space domain.

In practice, an exact Laplacian or second derivative would not be attempted

because it would infinitely amplify the noise. Instead, some numerical approximation to the derivative or an apodized frequency-domain filter (CHIU, BARRETT and SIMPSON [1980]) would be used, but the resulting space-domain filter would still be much more compact than in the 2D case.

3.5. SUMMARY IN OPERATOR FORM

The 3D Radon transform is described by the operator $\mathscr{R}_3$,

$$\lambda = \mathscr{R}_3\{f\}. \tag{3.22}$$

The 3D central-slice theorem (3.5) or (3.7) in operator notation is

$$\mathscr{F}_3 = \mathscr{F}_1 \mathscr{R}_3, \tag{3.23}$$

from which it follows that [cf. (3.9)]

$$\mathscr{R}_3^{-1} = \mathscr{F}_3^{-1} \mathscr{F}_1. \tag{3.24}$$

The summation image $b(r)$ is found by applying the operator $\mathscr{B}_3$ to the projection set as in (3.12), which becomes

$$b = \mathscr{B}_3\{\lambda\}. \tag{3.25}$$

With this operator, (3.10) and (3.11) may be written as

$$\mathscr{R}_3^{-1} = -\frac{1}{4\pi^2} \mathscr{B}_3 \frac{\partial^2}{\partial p^2}$$

$$= -\frac{1}{4\pi^2} \nabla^2 \mathscr{B}_3. \tag{3.26}$$

If it is desired to carry out the filtering in the frequency domain, as in (3.10) or (3.19), we write [cf. (2.54)]

$$\mathscr{R}_3^{-1} = \mathscr{B}_3 \mathscr{F}_1^{-1} v^2 \mathscr{F}_1 = \mathscr{F}_3^{-1} \sigma^2 \mathscr{F}_3 \mathscr{B}_3, \tag{3.27}$$

where v^2 and σ^2 are multiplicative operators in Fourier space.

§ 4. Related Transforms

4.1. THE GENERAL m-DIMENSIONAL RADON TRANSFORM

In the mathematical literature, considerable attention has been given to the general Radon transform in an m-dimensional Euclidean space. We shall briefly summarize this work here; for more detail, see DEANS [1983], LUDWIG [1966], JOHN [1955], HELGASON [1980], and COURANT and HILBERT [1962].

By analogy with (2.5) or (3.1), the m-dimensional (mD) Radon transform is defined by

$$\lambda_{\hat{n}}(p) = \int_{\infty} d^{m}r \, f(r)\delta(p - r \cdot \hat{n}), \qquad (4.1)$$

where r is the general mD position vector, $\hat{n}$ is an mD unit vector, and p is a scalar. Thus, $\delta(p - r \cdot \hat{n})$ is a 1D delta function that reduces the mD volume integral in (4.1) to an integral over the $(m - 1)$-dimensional hyperplane having the equation $p = r \cdot \hat{n}$. In operator form, (4.1) becomes

$$\lambda = \mathscr{R}_{m}\{f\}. \qquad (4.2)$$

The mD central-slice theorem is readily obtained by taking the 1D Fourier transform of (4.1), yielding

$$
\begin{aligned}
\Lambda_{\hat{n}}(v) &= \mathscr{F}_{1}\{\lambda_{\hat{n}}(p)\} \\
&= \int_{-\infty}^{\infty} dp \, e^{-2\pi i v p} \int_{\infty} d^{m}r \, f(r)\delta(p - r \cdot \hat{n}) \\
&= \int_{\infty} d^{m}r \, f(r)e^{-2\pi i r \cdot \hat{n} v} \\
&= F(\hat{n}v), \qquad (4.3)
\end{aligned}
$$

where $F(\rho)$ is the mD Fourier transform of $f(r)$. (Note that we are using the same notation in mD as in 2D.) Thus, once again, the 1D Fourier transform of a projection of a function yields one line through the mD transform of the function itself. The operator equivalent of (4.3) is [cf. (2.50) and (3.23)]:

$$\mathscr{F}_{m} = \mathscr{F}_{1}\mathscr{R}_{m}. \qquad (4.4)$$

The mD inverse Radon transform follows from an mD inverse Fourier transform of (4.3). As in §§ 2.3 and 3.3, we allow the frequency variable ρ to take on both positive and negative values, so that the general mD inverse

Fourier transform is

$$f(r) = \int_{-\infty}^{\infty} |\rho|^{m-1} \, d\rho \int_{\frac{1}{2}\omega_m} d\Omega_\rho F(\rho) \exp(2\pi i \rho \cdot r), \qquad (4.5)$$

where $d\Omega_\rho$ is the element of solid angle associated with the vector ρ, and ω_m, the solid angle subtended by a full sphere in the mD hyperspace, is given by (JOHN [1955])

$$\omega_m = \frac{2\sqrt{\pi^m}}{\Gamma(m/2)}. \qquad (4.6)$$

Note that $\omega_2 = 2\pi$ and $\omega_3 = 4\pi$ since $\Gamma(1) = 1$, and $\Gamma(3/2) = \sqrt{\pi}/2$.

We next let $\rho = \hat{n}v$, implying that $|\rho| = |v|$ and $d\Omega_\rho = d\Omega_n$. Combining (4.3) and (4.5) yields [cf. (3.9)]

$$f(r) = \mathcal{R}_m^{-1}\{\lambda\} = \int_{-\infty}^{\infty} |v|^{m-1} \, dv \int_{\frac{1}{2}\omega_m} d\Omega_n \Lambda_{\hat{n}}(v) \exp(2\pi i v r \cdot \hat{n}). \qquad (4.7)$$

At this point, a distinction must be made between odd and even m. For odd m, $|v|^{m-1} = v^{m-1}$, and the 1D Fourier derivative theorem (2.59) allows us to write [cf. (3.10)]

$$f(r) = \left(\frac{1}{2\pi i}\right)^{m-1} \int_{\frac{1}{2}\omega_m} d\Omega_n \left[\frac{\partial^{m-1}}{\partial p^{m-1}} \lambda_{\hat{n}}(p)\right]_{p = r \cdot \hat{n}}, \qquad (m \text{ odd}), \quad (4.8)$$

Thus, the mD inverse Radon transform in this case is implemented by differentiating each 1D projection $m - 1$ times, back-projecting (substituting $r \cdot \hat{n}$ for p), and integrating over all projection directions $\hat{n}$. In operator form [cf. (3.26)],

$$\mathcal{R}_m^{-1} = \left(\frac{1}{2\pi i}\right)^{m-1} \mathcal{B}_m \frac{\partial^{m-1}}{\partial p^{m-1}}, \qquad (m \text{ odd}), \qquad (4.9)$$

where $\mathcal{B}_m$ is the operator for mD back-projection and summation.

The case of even m is slightly more complicated because then $|v|^{m-1} = v^{m-1} \operatorname{sgn} v$. Multiplication of a 1D function by $\operatorname{sgn} v$ in the frequency domain is equivalent to $-i$ times the Hilbert transform operator $\mathcal{H}$ [see (2.27) and (2.53)] in the space domain. Hence,

$$\mathcal{R}_m^{-1} = -i\left(\frac{1}{2\pi i}\right)^{m-1} \mathcal{B}_m \mathcal{H} \frac{\partial^{m-1}}{\partial p^{m-1}}, \qquad (m \text{ even}). \qquad (4.10)$$

Explicitly,

$$f(r) = \frac{i}{\pi} \left(\frac{1}{2\pi i}\right)^{m-1} \int_{\frac{1}{2}\omega_m} d\Omega_n \left[\frac{1}{p} * \frac{\partial^{m-1} \lambda_{\hat{n}}(p)}{\partial p^{m-1}}\right]_{p = r \cdot \hat{n}}, \qquad (4.11)$$

$$(m \text{ even}),$$

where the Cauchy principal value of $1/p$ is understood. Many equivalent forms of (4.11) may be generated by integrating by parts.

The distinction between odd and even m is not necessary if the filtering is carried out in the frequency domain, and in both cases (4.7) becomes

$$\mathcal{R}_m^{-1} = \mathcal{B}_m \mathcal{F}_1^{-1} |v|^{m-1} \mathcal{F}_1. \qquad (4.12)$$

4.2. THE ABEL TRANSFORM AND ITS 3D GENERALIZATION

The Abel transform, designated by the operator $\mathcal{A}$, is a special case of the 2D Radon transform, valid when the function being transformed is rotationally symmetric. If a function $f(r)$ is independent of the polar angle θ in polar coordinates, $r = (r, \theta)$, then all projection directions are equivalent and we may as well take the vector $\hat{n}$ parallel to the x-axis. Then (2.4) becomes

$$\lambda(x) = \mathcal{R}_2\{f(r)\} = \mathcal{A}\{f(r)\} = \int_{-\infty}^{\infty} f(r) \, dy. \qquad (4.13)$$

Since $x^2 + y^2 = r^2$, we also have

$$\lambda(x) = 2 \int_{|x|}^{\infty} f(r) \frac{dy}{dr} dr = 2 \int_{|x|}^{\infty} \frac{f(r) r \, dr}{[r^2 - x^2]^{1/2}}, \qquad (4.14)$$

which is the explicit form of the Abel transform.

There are many ways to derive the inverse Abel transform. BRACEWELL [1965] makes a change of variables that reduces the integral in (4.14) to a convolution, which is then inverted by Fourier methods. It is also possible to carry out the ϕ integration in the general 2D inverse Radon transform (2.29) to get the inverse Abel transform. However, it is instructive to derive the inverse Abel transform directly from the central-slice theorem (BARRETT and SWINDELL [1981]). The operator form of the central-slice theorem (2.50) is

$$\mathcal{F}_2 = \mathcal{F}_1 \mathcal{R}_2. \qquad (4.15)$$

For rotationally symmetric functions, $\mathscr{F}_2$ is the zero-order Hankel operator $\mathscr{H}_0$ (not to be confused with the Hilbert operator $\mathscr{H}$), defined by

$$\mathscr{F}_2\{f(r)\} = \mathscr{H}_0\{f(r)\} = 2\pi \int_0^\infty r\,dr\,J_0(2\pi\rho r)f(r), \qquad (4.16)$$

and $\mathscr{R}_2 = \mathscr{A}$. Note that $\mathscr{H}_0^{-1} = \mathscr{H}_0$ (GASKILL [1978]). Therefore, (4.15) becomes

$$\mathscr{H}_0 = \mathscr{F}_1\,\mathscr{A}, \qquad (4.17)$$

from which it follows that

$$\mathscr{A}^{-1} = \mathscr{H}_0\,\mathscr{F}_1. \qquad (4.18)$$

Explicitly, since $\lambda(x) = \lambda(-x)$,

$$f(r) = \mathscr{A}^{-1}\{\lambda(x)\} = 2\pi \int_0^\infty \rho\,d\rho\,J_0(2\pi\rho r) \int_{-\infty}^\infty \lambda(x)\exp(-2\pi i\rho x)\,dx$$

$$= \int_0^\infty d\rho\,J_0(2\pi\rho r) \int_{-\infty}^\infty \lambda(x)\,2\pi\rho\cos(2\pi\rho x)\,dx$$

$$= \int_0^\infty d\rho\,J_0(2\pi\rho r) \int_{-\infty}^\infty \lambda(x)\frac{d}{dx}[\sin(2\pi\rho x)]\,dx$$

$$= -\frac{1}{\pi}\int_r^\infty \frac{d\lambda/dx}{(x^2-r^2)^{1/2}}\,dx, \qquad (r>0), \qquad (4.19)$$

where, in the last line, we have performed an integration by parts and made use of the integral,

$$\int_0^\infty J_0(at)\sin bt\,dt = \begin{cases} 0, & b<a \\ (b^2-a^2)^{-1/2}, & b>a. \end{cases} \qquad (4.20)$$

Note that the lower limit in the last form of (4.19) is r. Therefore, to find $f(r)$, one needs only the values of $\lambda(x)$ for $x > r$. EIN-GAL [1975] refers to this result as the *hole theorem*; a hole in Radon space of radius r does not preclude an exact reconstruction of $f(r)$. We shall see in § 4.3 that this theorem holds even if the object is not rotationally symmetric.

A very interesting situation arises when we consider the 3D Radon transform of a spherically symmetric function $f(r)$. We shall denote the special form of $\mathscr{R}_3$ in this case as $\mathscr{V}$, given by

$$\lambda(x) = \mathscr{R}_3\{f(r)\} = \mathscr{V}\{f(r)\} = \int_{-\infty}^\infty dy \int_{-\infty}^\infty dz\,f(r). \qquad (4.21)$$

Since $r^2 = x^2 + y^2 + z^2$, we can write

$$\int_{-\infty}^{\infty} dy \int_{-\infty}^{\infty} dz = 2\pi \int_0^{\infty} u\,du = 2\pi \int_{|x|}^{\infty} r\,dr, \qquad (4.22)$$

where $u^2 = y^2 + z^2$. Thus

$$\lambda(x) = 2\pi \int_{|x|}^{\infty} r\,dr\,f(r). \qquad (4.23)$$

Straightforward differentiation then shows that

$$\frac{d\lambda(x)}{dx} = -2\pi x\,f(x), \qquad (4.24)$$

or

$$f(r) = \mathcal{V}^{-1}\{\lambda(x)\} = -\frac{1}{2\pi r}\lambda'(r) \qquad (4.25)$$

where $\lambda'(r) = d\lambda(r)/dr$. In this case, *the inverse transform is not an integral transform at all, but just a simple derivative.* Back-projection is not required, and only projection values in the neighborhood of a single point in Radon space are required to determine $f(r)$ for a particular r.

This remarkable result is related to the local nature of the filtering operation in the 3D inverse Radon transform. Indeed, if $\lambda_{\hat{n}}(p)$ is independent of $\hat{n}$, (3.10) becomes (CHIU, BARRETT and SIMPSON [1980])

$$f(r) = -\frac{1}{4\pi^2} \cdot 2\pi \int_0^1 d(\cos\theta_n)\,\lambda''(r\cos\theta_n)$$

$$= -\frac{1}{2\pi r}\int_0^r dt\,\lambda''(t) = -\frac{1}{2\pi r}\lambda'(r) \qquad (4.26)$$

where $t = r\cos\theta_n$ and $\lambda'(0) = 0$, since λ is an even, differentiable function. Equation (4.26) agrees with (4.25), showing directly that $\mathcal{R}_3^{-1}$ reduces to $\mathcal{V}^{-1}$ for spherical symmetry.

Equation (4.25) was first given in the optics literature by VEST and STEEL [1978], but it was known much earlier in the literature on Compton scattering [DuMOND, 1929] and positron annihilation (STEWART [1957]; MIJNARENDS [1967]).

4.3. THE CORMACK TRANSFORM

Although RADON [1917] had laid the mathematical groundwork for reconstruction from projections, his work was not widely known and its importance to radiological imaging was not recognized until the late 1960s. An independent and mathematically rigorous formulation was obtained by CORMACK [1963, 1964], and this work may properly be regarded as the beginning of modern computed tomography.

Cormack's approach was to recognize that, in polar coordinates, any physically meaningful function $f(r, \theta)$ is periodic in θ with period 2π. Therefore, it can be expanded in a Fourier series or *circular harmonic decomposition* of the form

$$f(r, \theta) = \sum_{l=-\infty}^{\infty} f_l(r)\, e^{il\theta}, \qquad (4.27)$$

where

$$f_l(r) = \frac{1}{2\pi} \int_0^{2\pi} f(r, \theta)\, e^{-il\theta}\, d\theta. \qquad (4.28)$$

Similarly, the projection $\lambda(p, \phi)$ can be expanded as

$$\lambda(p, \phi) = \sum_{l=-\infty}^{\infty} \lambda_l(p)\, e^{il\phi}, \qquad (4.29)$$

with

$$\lambda_l(p) = \frac{1}{2\pi} \int_0^{2\pi} \lambda(p, \phi)\, e^{-il\phi}\, d\phi. \qquad (4.30)$$

(Note the slight change in notation from § 2; $\lambda_l(p)$ should not be confused with $\lambda_\phi(p)$, which is now denoted $\lambda(p, \phi)$.) By the same token, the 2D Fourier transform $F(\rho, \theta_\rho)$ of $f(r, \theta)$ may be written

$$F(\rho, \theta_\rho) = \sum_{l=-\infty}^{\infty} F_l(\rho)\, e^{il\theta_\rho}, \qquad (4.31)$$

where

$$F_l(\rho) = \frac{1}{2\pi} \int_0^{2\pi} F(\rho, \theta_\rho)\, e^{-il\theta_\rho}\, d\theta_\rho. \qquad (4.32)$$

We have already explored in some detail the relationships among $f(r, \theta)$, $F(\rho, \theta_\rho)$, and $\lambda(p, \phi)$, which are summarized in the operator equations (2.47),

(2.50), and (2.51). In this section, we derive the corresponding relationships connecting $f_\ell(\theta)$, $F_\ell(\theta_\rho)$, and $\lambda_\ell(\phi)$. The development here follows CHIU [1980].

Let us first investigate the relationship between $f_\ell(r)$ and $F_\ell(\rho)$. The 2D Fourier transform of $f(r, \theta)$ is given by

$$F(\rho, \theta_\rho) = \int_0^\infty r\, dr \int_0^{2\pi} d\theta\, f(r, \theta) \exp[-2\pi i \rho r \cos(\theta - \theta_\rho)], \quad (4.33)$$

which, with (4.27) and (4.31), becomes

$$\sum_{\ell=-\infty}^\infty F_\ell(\rho)\, e^{i\ell\theta_\rho} = \sum_{\ell=-\infty}^\infty e^{i\ell\theta_\rho} \int_0^\infty r\, dr \int_0^{2\pi} d\theta\, e^{i\ell(\theta-\theta_\rho)}$$
$$\times \exp[-2\pi i \rho r \cos(\theta - \theta_\rho)]\, f_\ell(r). \quad (4.34)$$

Since the functions $\exp(i\ell\theta_\rho)$ form a complete, orthogonal set on $0 < \theta_\rho \leq 2\pi$, (4.34) must hold term by term, i.e.

$$F_\ell(\rho) = \int_0^\infty r\, dr \int_0^{2\pi} d\psi\, e^{i\,\ell\psi} \exp(-2\pi i \rho r \cos\psi) f_\ell(r) \quad (4.35)$$

where $\psi = \theta - \theta_\rho$. We recognize the integral over ψ as a standard representation of the Bessel function of order ℓ:

$$J_\ell(z) = \frac{(-i)^\ell}{2\pi} \int_0^{2\pi} e^{i\ell\psi} e^{-iz\cos\psi}\, d\psi. \quad (4.36)$$

Hence,

$$F_\ell(\rho) = 2\pi i^\ell \int_0^\infty r\, dr\, f_\ell(r) J_\ell(2\pi\rho r) = i^\ell \mathscr{H}_\ell\{f_\ell(r)\}, \quad (4.37)$$

where $\mathscr{H}_\ell$ is the operator for the ℓth-order Hankel transform. Thus $f_\ell(r)$ and $F_\ell(\rho)$ form an ℓth-order Hankel-transform pair. Since the Hankel transform is self-inverse, i.e. $\mathscr{H}_\ell^{-1} = \mathscr{H}_\ell$, we also have

$$f_\ell(r) = (-i)^\ell \mathscr{H}_\ell\{F_\ell(\rho)\}. \quad (4.38)$$

We already know from the central-slice theorem that $F(\rho, \theta_\rho)$ is the 1D Fourier transform of $\lambda(p, \phi)$ if we set $v = \rho$ and $\phi = \theta_\rho$. In terms of circular harmonics,

$$\mathscr{F}_1\{\lambda(p, \phi)\} = \int_{-\infty}^\infty dp\, e^{-2\pi i v p} \sum_\ell \lambda_\ell(p)\, e^{i\ell\phi} = \sum_\ell F_\ell(v)\, e^{i\ell\phi}. \quad (4.39)$$

Again, this equation must hold term by term, and we see that $\lambda_\ell(p)$ and $F_\ell(v)$ are a 1D Fourier-transform pair, written symbolically as

$$F_\ell(v) = \mathscr{F}_1\{\lambda_\ell(p)\}. \tag{4.40}$$

We now know the operators connecting f_ℓ with F_ℓ and λ_ℓ with F_ℓ. All that remains is to find the connection between λ_ℓ and f_ℓ, which we refer to as the Cormack transform of order ℓ and denote by the operator $\mathscr{C}_\ell$:

$$\lambda_\ell(p) = \mathscr{C}_\ell\{f_\ell(r)\}. \tag{4.41}$$

From the definition of the Radon transform, (2.5), we have

$$\lambda(p, \phi) = \int_0^\infty r\,dr \int_0^{2\pi} d\theta\, f(r, \theta)\delta[p - r\cos(\theta - \phi)]. \tag{4.42}$$

Using the circular harmonic expansions (4.27) and (4.28) and again invoking the orthogonality of the harmonics, we get

$$\lambda_\ell(p) = \int_0^\infty r\,dr\, f_\ell(r) \int_0^{2\pi} d\psi\, e^{i\ell\psi}\delta(p - r\cos\psi), \tag{4.43}$$

where $\psi = \theta - \phi$. The ψ integral may be performed by steps similar to those leading to (2.42) (CHIU [1980]), and the result is

$$\lambda_\ell(p) = 2\int_{|p|}^\infty r\,dr\, f_\ell(r) \frac{\cos[\ell\cos^{-1}(p/r)]}{(r^2 - p^2)^{1/2}}$$

$$= 2\int_{|p|}^\infty r\,dr \frac{f_\ell(r)T_\ell(p/r)}{(r^2 - p^2)^{1/2}} = \mathscr{C}_\ell\{f(r)\}, \tag{4.44}$$

where $T_\ell(p/r)$ is the Tschebycheff polynomial of the first kind of order ℓ, defined by

$$T_\ell(x) = \begin{cases} \cos(\ell\cos^{-1}x), & |x| < 1 \\ \cosh(\ell\cosh^{-1}x), & |x| > 1. \end{cases} \tag{4.45}$$

For a thorough but very readable introduction to these polynomials, see VAN DER POL and WEIJERS [1934].

Note that if $f(r, \theta)$ is rotationally symmetric, $f_\ell(r)$ is non-zero only for $\ell = 0$; in this case (4.44) reduces to the Abel transform (4.14) since $T_0(u) = 1$ for all u.

To gain more insight into the Cormack transform, let us consider a specific object, namely a cylindrical shell of radius R with an azimuthal dependence

given by $\cos k\theta$ (k integer). That is, $f(r, \theta) = \delta(r - R)\cos k\theta$. By (4.28), the circular-harmonic decomposition of this object is

$$f_\ell(r) = \tfrac{1}{2}\delta(r - R)[\delta_{\ell,k} + \delta_{\ell,-k}], \qquad (4.46)$$

where $\delta_{\ell,k}$ is the usual Kronecker symbol. From (4.44),

$$\lambda_\ell(p) = \frac{R}{(R^2 - p^2)^{1/2}}\left[T_k\left(\frac{p}{R}\right) + T_{-k}\left(\frac{p}{R}\right)\right],$$

$$= \frac{2R}{(R^2 - p^2)^{1/2}}T_k\left(\frac{p}{R}\right), \qquad |p| < R, \qquad (4.47)$$

where the last step follows because $T_k(u) = T_{-k}(u)$ for all k and u. The factor $(R^2 - p^2)^{-1/2}$ in (4.47) represents the projection of the cylindrical shell $\delta(r - R)$, as illustrated in Fig. 5a, while $T_k(p/R)$ is the projection of $\cos k\theta$ (Fig. 5b). A general object can then be constructed as a superposition of cylindrical shells with various radii and azimuthal frequencies, and its projection is a superposition of terms like (4.47).

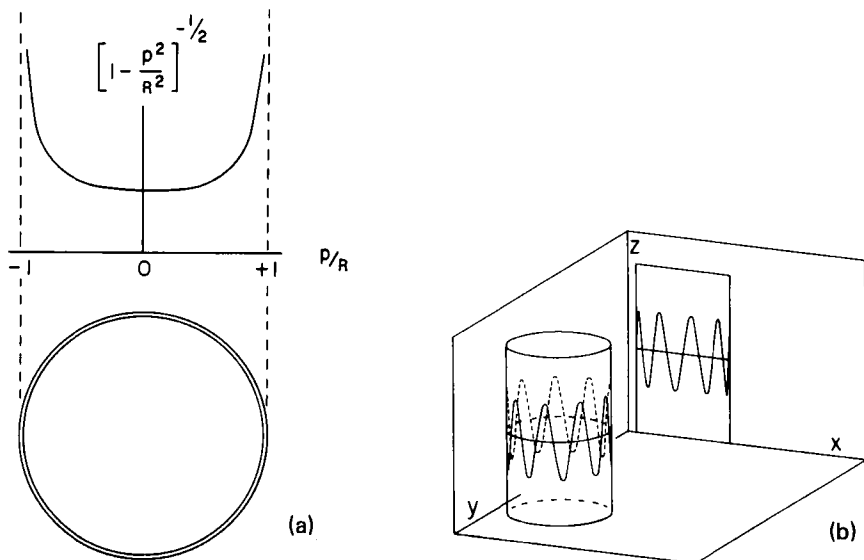The Tschebycheff polynomial may also be visualized as a Lissajous pattern

Fig. 5. (a) The projection of a thin circular shell $\delta(r - R)$ is $(R^2 - p^2)^{-1/2}$. (b) The projection of $\cos k\theta$ is $T_k(p/R)$. (After VAN DER POL and WEIJERS [1934].)

between two cosine waves having frequencies in the ratio $k : 1$ (VAN DER POL and WEIJERS [1934]). If the y-axis of an oscilloscope is driven with a voltage $\cos k\omega t$ and the x-axis is driven with $\cos \omega t$, then the display is

$$y = \cos(k \cos^{-1} x) = T_k(x). \tag{4.48}$$

Exactly the same cosine distortion of the x-axis occurs when the function $\cos k\theta$ is projected from a cylinder to a plane.

There are many ways to derive the inverse Cormack transform. Cormack himself used the orthogonality properties of the Tschebycheff polynomials. EIN-GAL [1975], HANSEN [1981], and VERLY [1982] used the Mellin transform, and CHIU [1980] and HAWKINS [1982] performed a tedious contour integration. We shall approach the problem by using operator algebra. From (4.41),

$$f_\ell(r) = \mathscr{C}_\ell^{-1}\{\lambda_\ell(p)\}, \tag{4.49}$$

while, from (4.38) and (4.40),

$$\begin{aligned} f_\ell(r) &= (-\mathrm{i})^\ell \mathscr{H}_\ell\{F_\ell(\rho)\} \\ &= (-\mathrm{i})^\ell \mathscr{H}_\ell \mathscr{F}_1\{\lambda_\ell(p)\}. \end{aligned} \tag{4.50}$$

Therefore (EIN-GAL [1975]),

$$\mathscr{C}_\ell^{-1} = (-\mathrm{i})^\ell \mathscr{H}_\ell \mathscr{F}_1. \tag{4.51}$$

To convert this result to an explicit integral transform, we use the definitions of $\mathscr{H}_\ell$ and $\mathscr{F}_1$, (4.37) and (2.9) respectively, to obtain

$$f_\ell(r) = (-\mathrm{i})^\ell 2\pi \int_0^\infty v\, \mathrm{d}v J_\ell(2\pi vr) \int_{-\infty}^\infty \mathrm{d}p\, \mathrm{e}^{-2\pi \mathrm{i}pv}\lambda_\ell(p). \tag{4.52}$$

From (2.14) and (4.30), it follows that $\lambda_\ell(p)$ is an even (odd) function of p if ℓ is even (odd), i.e.

$$\lambda_\ell(-p) = (-1)^\ell \lambda_\ell(p). \tag{4.53}$$

Therefore, only the term proportional to $\cos(2\pi pv)$ contributes to the p integral in (4.52) for ℓ even, while only the term in $\sin(2\pi pv)$ contributes for ℓ odd. We can rewrite (4.52) as

$$f_\ell(r) = 2(-\mathrm{i})^\ell \int_0^\infty \mathrm{d}p\, \lambda_\ell(p) \frac{\partial I_\ell(p, r)}{\partial p}, \tag{4.54}$$

where

$$
I_\ell(p, r) = \begin{cases} \displaystyle\int_0^\infty \mathrm{d}v\, J_\ell(2\pi v r)\sin(2\pi p v), & \ell \text{ even}, \\[2ex] \displaystyle i\int_0^\infty \mathrm{d}v\, J_\ell(2\pi v r)\cos(2\pi p v), & \ell \text{ odd}. \end{cases} \tag{4.55}
$$

From tabulated integrals and properties of the Tschebycheff polynomials (GRADSHTEYN and RYZHIK [1980], pp. 730 and 1032; VAN DER POL and WEIJERS [1934]), we find

$$
I_\ell(p, r) = \begin{cases} \dfrac{-i^\ell}{2\pi r} U_{\ell-1}\left(\dfrac{p}{r}\right) & r > p > 0, \\[2ex] \dfrac{i^\ell}{2\pi r}\left[\dfrac{T_\ell(p/r)}{[(p^2/r^2)-1]^{1/2}} - U_{\ell-1}\left(\dfrac{p}{r}\right)\right], & p > r > 0 \end{cases} \tag{4.56}
$$

where $U_\ell(x)$ is the Tschebycheff polynomial of the second kind, defined by

$$
U_\ell(x) = \begin{cases} \sin[(\ell+1)\cos^{-1}x]/\sin(\cos^{-1}x), & x < 1 \\[1ex] \sinh[(\ell+1)\cosh^{-1}x]/\sinh(\cosh^{-1}x), & x > 1. \end{cases} \tag{4.57}
$$

With (4.56) and an integration by parts, (4.54) becomes

$$
f_\ell(r) = -\frac{1}{\pi}\int_r^\infty \mathrm{d}p\,\frac{\lambda_\ell'(p)T_\ell(p/r)}{(p^2-r^2)^{1/2}} + \frac{1}{\pi r}\int_0^\infty \mathrm{d}p\,\lambda_\ell'(p)U_{\ell-1}(p/r). \tag{4.58}
$$

The second integral in (4.58) is actually zero. The proof of this contention (CHIU [1980]) rests on the fact that $U_\ell(x)$ is a polynomial of degree ℓ, and on the consistency condition, to be discussed below, which states that (CORMACK [1963]; EIN-GAL [1975]; VERLY [1981])

$$
\int_0^\infty \lambda_\ell(p)p^k\,\mathrm{d}p = 0, \tag{4.59}
$$

for $0 < k < |\ell|$ and $k + |\ell|$ even. Therefore, the final form of the inverse Cormack transform is

$$
f_\ell(r) = \mathscr{C}_\ell^{-1}\{\lambda_\ell\} = -\frac{1}{\pi}\int_r^\infty \mathrm{d}p\,\frac{\lambda_\ell'(p)T_\ell(p/r)}{(p^2-r^2)^{1/2}}, \qquad (r > 0). \tag{4.60}
$$

An interesting feature of this result is that only values of $\lambda(p)$ for $p > |r|$ are required to reconstruct $f(r)$ (LEWITT and BATES [1978]). This is again the hole

theorem (EIN-GAL [1975]), discussed for rotationally symmetric functions below (4.20). Note also that $\mathscr{C}_0^{-1} = \mathscr{A}^{-1}$ [cf. (4.19) and (4.60)] since $T_0(x) = 1$.

We now derive the consistency condition (4.59). The derivation given here follows CHIU [1980].

From (2.39), a point object has as its projection the 1D delta function $\delta(p - r \cdot n)$. Since a more general object can be considered as a superposition of points, it will suffice to show that the consistency relation holds when $\lambda(p, \phi) = \delta(p - r \cdot \hat{n})$. In other words, if we can show that

$$\int_0^\infty p^k \, dp \int_0^{2\pi} d\phi \, \delta(p - r \cdot \hat{n}) e^{-i\ell\phi} = 0 \tag{4.61}$$

for certain values of k and ℓ, then we can be guaranteed, by the principle of linear superposition, that (4.59) holds for the same values of k and ℓ.

Interchanging the order of integration in (4.61), we get

$$\int_0^{2\pi} d\phi \int_0^\infty p^k \, dp \, e^{-i\ell\phi} \delta[p - r\cos(\theta - \phi)]$$

$$= e^{-i\ell\theta} \int_0^{2\pi} d\psi \, e^{i\ell\psi} \int_0^\infty p^k \, dp \, \delta(p - r\cos\psi)$$

$$= e^{-i\ell\theta} \int_{-\pi/2}^{\pi/2} d\psi \, e^{i\ell\psi} (r\cos\psi)^k$$

$$= r^k e^{-i\ell\theta} \int_{-\pi/2}^{\pi/2} d\psi \cos\ell\psi \, (\cos\psi)^k$$

$$= \left(\frac{r}{2}\right)^k e^{-i\ell\theta} \int_{-\pi/2}^{\pi/2} d\psi \, [e^{i(k-\ell)\psi} + k e^{i(k-\ell-2)\psi} + \ldots$$
$$+ e^{i(-k-\ell)\psi}], \tag{4.62}$$

where $\psi = \theta - \phi$. Every term will vanish if $k - \ell, k - \ell - 2, \ldots, -k - \ell$ are all nonzero even numbers. This occurs if $k + |\ell|$ is even and $0 \le k < |\ell|$, and, under these conditions, (4.61) and (4.59) must hold.

The consistency condition is of considerable theoretical importance because several different forms of the inverse Cormack transform appear in the literature. An example of two apparently different forms is (4.58) and (4.60). However, in this case as well as many others, application of the consistency condition removes the discrepancy (VERLY [1981]).

There are several other mathematical subtleties related to the stability and uniqueness of the inverse Cormack transform. For a thorough review, see HAWKINS [1982].

4.4. THE GEGENBAUER TRANSFORM

Just as the 2D functions $f(r, \theta)$, $\lambda(p, \phi)$, and $F(\rho, \theta_\rho)$ can be expanded in circular harmonics, so too can the corresponding 3D functions be expanded in spherical harmonics. The 3D counterpart of the Cormack transform is called the Gegenbauer transform. A brief survey of this theory is given here. For more details, see LUDWIG [1966], CHIU [1980], HAWKINS [1982], and DEANS [1983].

A 3D object in spherical coordinates, $f(r, \theta, \phi)$, can be expanded as

$$f(r, \theta, \phi) = \sum_{l=0}^{\infty} \sum_{m=-l}^{l} f_{lm}(r) Y_{lm}(\theta, \phi), \qquad (4.63)$$

where $Y_{lm}(\theta, \phi)$ is a spherical harmonic (JACKSON [1975]). The expansion coefficient $f_{lm}(r)$ is given by

$$f_{lm}(r) = \int_0^{2\pi} \mathrm{d}\phi \int_0^{\pi} \mathrm{d}\theta \sin\theta f(r, \theta, \phi) Y^*_{lm}(\theta, \phi). \qquad (4.64)$$

The projection data, $\lambda_\theta(p) = \lambda(p, \theta_n, \phi_n)$, and the 3D Fourier transform of the object, $F(\sigma, \theta_\sigma, \phi_\sigma)$, have similar expansions:

$$\lambda(p, \theta_n, \phi_n) = \sum_{l,m} \lambda_{lm}(p) Y_{lm}(\theta_n, \phi_n), \qquad (4.65)$$

$$F(\sigma, \theta_\sigma, \phi_\sigma) = \sum_{l,m} F_{lm}(\sigma) Y_{lm}(\theta_\sigma, \phi_\sigma), \qquad (4.66)$$

with inverses analogous to (4.64).

The relation between $f_{lm}(r)$ and $F_{lm}(\sigma)$ is (CHIU [1980])

$$F_m(\sigma) = i^l \mathcal{J}_l \{f_{lm}(r)\}, \qquad (4.67)$$

where $\mathcal{J}_l$ is the operator for the lth-order spherical Bessel transform, given by [cf. (4.37)]

$$\mathcal{J}_l \{f_{lm}(r)\} = 4\pi \int_0^{\infty} f_{lm}(r) j_l(2\pi\sigma r) r^2 \, \mathrm{d}r, \qquad (4.68)$$

where $j_l(u)$ is the spherical Bessel function of the first kind, which is related to the ordinary Bessel function by (MORSE and FESHBACH [1953] p. 1573)

$$j_l(u) = (\pi/2u)^{1/2} J_{l+1/2}(u). \qquad (4.69)$$

Since $\mathcal{J}_l^{-1} = \mathcal{J}_l$ (MORSE and FESHBACH [1953] p. 781), we also have

$$f_{lm}(r) = (-i)^l \mathcal{J}_l \{F_{lm}(\sigma)\}. \qquad (4.70)$$

If the object is spherically symmetric, the only nonzero harmonic is $\ell = m = 0$, and

$$F(\sigma) = 4\pi \int_0^\infty f(r)\,\text{sinc}\,(2\sigma r)r^2\,\mathrm{d}r, \tag{4.71}$$

$$f(r) = 4\pi \int_0^\infty F(\sigma)\,\text{sinc}\,(2\sigma r)\sigma^2\,\mathrm{d}\sigma, \tag{4.72}$$

since

$$j_0(\pi u) = \frac{\sin \pi u}{\pi u} \equiv \text{sinc}\,(u). \tag{4.73}$$

From a spherical-harmonic decomposition of the 3D-central-slice theorem, (3.7) or (3.23), it follows readily that $\lambda_{\ell m}(p)$ and $F_{\ell m}(\sigma)$ are a 1D Fourier-transform pair, i.e. [cf. (4.40)]

$$F_{\ell m}(\sigma) = \mathscr{F}_1\{\lambda_{\ell m}(p)\}. \tag{4.74}$$

The remaining relation that is needed is the one connecting $f_{\ell m}(r)$ and $\lambda_{\ell m}(p)$. This relation is called the 3D Gegenbauer transform of order ℓ, and is denoted by the operator $\mathscr{G}_{3,\ell}$, so that

$$\lambda_{\ell m}(p) = \mathscr{G}_{3,\ell}\{f_{\ell m}(r)\}. \tag{4.75}$$

Explicitly (LUDWIG [1966]; CHIU [1980]):

$$\lambda_{\ell m}(p) = 2\pi \int_{|p|}^\infty f_{\ell m}(r)P_\ell(p/r)r\,\mathrm{d}r, \tag{4.76}$$

where P_ℓ is the Legendre polynomial.

The inverse Gegenbauer transform is given by

$$f_{\ell m}(r) = \mathscr{G}_{3,\ell}^{-1}\{\lambda_{\ell m}(p)\} = -\frac{1}{2\pi r}\int_0^r \lambda''_{\ell m}(p)P_\ell(p/r)\,\mathrm{d}p. \tag{4.77}$$

Note that $\mathscr{G}_{3,\ell}$ is independent of m.

If the object is spherically symmetric, (4.77) reduces to

$$f(r) = -\frac{1}{2\pi r}\int_0^r \lambda''(p)\,\mathrm{d}p = -\frac{1}{2\pi r}\lambda'(r), \tag{4.78}$$

which is just the VEST–STEEL relation (4.25). Thus (CHIU [1980])

$$\mathscr{G}_{3,0}^{-1} = \mathscr{V}^{-1}. \tag{4.79}$$

The m-dimensional generalization of these results has been given by LUDWIG [1966].

4.5. THE DIPOLE-SHEET TRANSFORM

The dipole-sheet transform (BARRETT [1982a]) is a symmetrized version of the 3D Radon transform. To see the asymmetry between the Radon transform and its inverse, let us rewrite (3.1) and (3.10) as

$$f_R(\boldsymbol{p}) = \mathcal{R}_3\{f(\boldsymbol{r})\} = \int_\infty d^3r\, f(\boldsymbol{r})\delta(p - \boldsymbol{r}\cdot\hat{\boldsymbol{n}}), \qquad (4.80)$$

$$f(\boldsymbol{r}) = \mathcal{R}_3^{-1}\{f_R(\boldsymbol{p})\} = -\frac{1}{4\pi^2}\int_\infty d^3p\, f_R(\boldsymbol{p})\delta''(p - \boldsymbol{r}\cdot\hat{\boldsymbol{n}})/p^2, \quad (4.81)$$

where $f_R(\boldsymbol{p})$ is what we have previously called $\lambda(p)$ or $\lambda_{\hat{n}}(p)$. The equivalence of (4.81) and (3.10) follows since $d^3p = p^2\,dp\,d\Omega_n$ and since the delta function has the effect of removing the p integration in (4.81), taking the second derivative of f_R with respect to p, and making the substitution $p = \boldsymbol{r}\cdot\hat{\boldsymbol{n}}$.

Comparing the forward and inverse transforms in this form, we see that they involve the same kernel $\delta(p - \boldsymbol{r}\cdot\hat{\boldsymbol{n}})$, but that the inverse transform includes the second-derivative operation, the factor $1/p^2$, and the constant $-1/(4\pi^2)$. A symmetrical transform pair results if we move one derivative and a factor of $i/(2\pi p)$ to the forward transform. Thus, we define a new transform pair by

$$f_D(\boldsymbol{p}) = \mathcal{D}\{f(\boldsymbol{r})\} = \int_\infty d^3r\, \psi(\boldsymbol{p}, \boldsymbol{r})f(\boldsymbol{r}), \qquad (4.82)$$

$$f(\boldsymbol{r}) = \mathcal{D}^{-1}\{f_D(\boldsymbol{p})\} = \int_\infty d^3p\, \psi^*(\boldsymbol{p}, \boldsymbol{r})f_D(\boldsymbol{p}), \qquad (4.83)$$

where the asterisk denotes complex conjugate, and

$$\psi(\boldsymbol{p}, \boldsymbol{r}) \equiv \frac{i}{2\pi p}\,\delta'(p - \boldsymbol{r}\cdot\hat{\boldsymbol{n}}). \qquad (4.84)$$

Regarded as a function of $\boldsymbol{r}$, the basis function $\psi(\boldsymbol{p}, \boldsymbol{r})$ vanishes except in an infinitesimal neighborhood of the plane $p = \boldsymbol{r}\cdot\hat{\boldsymbol{n}}$. It takes on the value $+i\infty$ just to one side of this plane and $-i\infty$ just to the other side of it. Physically, $\psi(\boldsymbol{p}, \boldsymbol{r})$ may be interpreted as a double layer or dipole sheet, and we refer to (4.82) as the dipole-sheet transform.

To derive the inverse dipole-sheet transform (4.83) from the inverse Radon transform, we note that

$$f_D(p) = \frac{i}{2\pi p} \frac{\partial}{\partial p} f_R(p), \qquad (4.85)$$

which follows by differentiating (4.80) under the integral sign. Next, we insert (4.85) into (4.81), yielding

$$f(r) = \frac{1}{4\pi^2} \int_{-\infty}^{\infty} dp \int_{2\pi} d\Omega_n \left[\frac{\partial f_R(p)}{\partial p} \right] \delta'(p - r \cdot \hat{n})$$

$$= -\frac{i}{2\pi} \int_{-\infty}^{\infty} dp \int_{2\pi} d\Omega_n p f_D(p) \delta'(p - r \cdot \hat{n})$$

$$= -\frac{i}{2\pi} \int_{\infty} d^3 p f_D(p) \delta'(p - r \cdot \hat{n})/p, \qquad (4.86)$$

in agreement with (4.83).

The functions $\psi(p, r)$ are orthonormal and complete (BARRETT [1982a]). That is,

$$\int_{\infty} \psi^*(p, r) \psi(p', r) \, d^3 r = \delta(p - p'), \qquad (4.87)$$

$$\int_{\infty} \psi^*(p, r) \psi(p, r') \, d^3 p = \delta(r - r'). \qquad (4.88)$$

The inverse transform (4.83) can also be derived by multiplying (4.82) by $\psi^*(p, r')$, integrating over p, and using (4.88).

The following identities, given here without proof, are useful in manipulating the dipole-sheet transform:

$$\delta^{(n)}(x) = (-1)^n n! x^{-n} \delta(x), \qquad (4.89)$$

$$\delta'(ax) = \frac{\delta'(x)}{a|a|}, \qquad (4.90)$$

$$-\frac{1}{8\pi^2} \int_{4\pi} d\Omega_n \delta''(r \cdot \hat{n}) = \delta(r), \qquad (4.91)$$

$$\int_{4\pi} d\Omega_n \delta(r \cdot p) = \int_{4\pi} d\Omega \delta(r \cdot p) = \frac{2\pi}{|rp|}, \qquad (4.92)$$

$$\int_{4\pi} d\Omega_n \, \delta(p - r \cdot \hat{n}) = \int_{4\pi} d\Omega \, \delta(p - r \cdot \hat{n}) = \frac{2\pi}{|r|} \text{rect}\left(\frac{p}{2r}\right), \quad (4.93)$$

$$\int_\infty d^3p \, \delta(p - r \cdot \hat{n}) = \frac{2\pi r^2}{3}, \quad (4.94)$$

$$\int_{4\pi} d\Omega_n \, \delta'(p - r \cdot \hat{n})$$

$$= \int_{4\pi} d\Omega \, \delta'(p - r \cdot \hat{n}) = \frac{-2\pi}{|r|} [\delta(p - |r|) - \delta(p + |r|)], \quad (4.95)$$

$$\int_{4\pi} d\Omega_n (r \cdot \hat{n})^2 \, \delta''(r \cdot \hat{n}) = \frac{4\pi}{|r|}, \quad (4.96)$$

$$\nabla^2 \frac{1}{|r|} = -4\pi\delta(r), \quad (4.97)$$

$$\nabla^2 f(r \cdot \hat{n}) = f''(r \cdot \hat{n}). \quad (4.98)$$

Here, $\delta^{(n)}(x)$ denotes the nth derivative of a 1D delta function, and the vectors p and r have magnitudes $|p|$ and $|r|$, respectively, but p and r can be positive or negative. Recall also that $\delta(r)$ is a 3D delta function, while $\delta(r)$ is 1D.

Identity (4.89) can be used to derive an interesting theorem for derivatives of the Radon transform. Using (4.89) with $n = 1$ in (4.92) yields

$$f_D(p) = \frac{-i}{2\pi p} \int_\infty d^3r f(r) \frac{\delta(p - r \cdot \hat{n})}{p - r \cdot \hat{n}} = \frac{-i}{2\pi p} \mathcal{R}_3 \left\{ \frac{f(r)}{p - r \cdot \hat{n}} \right\}, \quad (4.99)$$

or, with (4.85)

$$-\frac{\partial}{\partial p} \mathcal{R}_3 \{ f(r) \} = \mathcal{R}_3 \left\{ \frac{f(r)}{p - r \cdot \hat{n}} \right\}. \quad (4.100)$$

This theorem is easily extended to the kth derivative of the mD Radon transform. Differentiating (4.1) and using (4.89) yields

$$\frac{\partial^k}{\partial p^k} \mathcal{R}_m \{ f(r) \} = (-1)^k k! \, \mathcal{R}_m \left\{ \frac{f(r)}{(p - r \cdot \hat{n})^k} \right\}, \quad (4.101)$$

where $(p - r \cdot \hat{n})^{-k}$ must be interpreted as a generalized function (Cauchy principal value for $k = 1$). Other formulas involving derivatives of the Radon transform are given by DEANS [1983].

The dipole sheet transform is very simple for spherically symmetric functions. Using identity (4.95) in (4.82) gives

$$f_D(p) = \frac{i}{2\pi p} \int_0^\infty r^2 \, dr f(r) \int_{4\pi} d\Omega \, \delta'(p - r \cdot \hat{n})$$

$$= \frac{i}{2\pi p} \int_0^\infty r^2 \, dr f(r) \left(\frac{-2\pi}{r}\right) \delta(p - r)$$

$$= -i f(p). \tag{4.102}$$

Thus, except for the factor $-i$, a spherically symmetric function is unchanged by the dipole-sheet transform. Any spherically symmetric function is an eigenfunction of $\mathscr{D}$.

Equation (4.102) is equivalent to the VEST–STEEL relation (4.25). From (4.85) and (4.102), we have

$$f_D(p) = \frac{i}{2\pi p} \frac{d}{dp} f_R(p) = -i f(p), \tag{4.103}$$

which is just (4.25).

From a mathematical point of view, the dipole-sheet transform is interesting because it is unitary, which means that its adjoint is the same as its inverse. For a general Hilbert-space operator $\mathcal{O}$, the adjoint $\mathcal{O}^\dagger$ is defined by

$$\langle u, \mathcal{O}v \rangle = \langle \mathcal{O}^\dagger u, v \rangle, \tag{4.104}$$

where u and v are vectors in the space and $\langle u, v \rangle$ denotes a scalar product. If u and v are represented as functions of r,

$$\langle u, v \rangle = \int_\infty d^3 r \, u^*(r) v(r). \tag{4.105}$$

If $\mathscr{D}$ is unitary, then

$$\langle \mathscr{D}u, \mathscr{D}v \rangle = \langle \mathscr{D}^\dagger \mathscr{D}u, v \rangle = \langle \mathscr{D}^{-1} \mathscr{D}u, v \rangle = \langle u, v \rangle, \tag{4.106}$$

or

$$\int_\infty d^3 p \, u_D^*(p) v_D(p) = \int_\infty d^3 r \, u^*(r) v(r), \tag{4.107}$$

which is analogous to Parseval's theorem in Fourier theory. To prove (4.107),

we simply express $u_D^*(\boldsymbol{p})$ and $v_D(\boldsymbol{p})$ by (4.82) and use (4.88), yielding

$$
\begin{aligned}
\langle \mathscr{D}u, \mathscr{D}v \rangle &= \int_\infty d^3p \int_\infty d^3r \int_\infty d^3r' \; \psi^*(\boldsymbol{p}, r)u^*(r)\psi(\boldsymbol{p}, r')v(r') \\
&= \int_\infty d^3r \int_\infty d^3r' \; \delta(r - r')u^*(r)v(r') \\
&= \int_\infty d^3r\, u^*(r)v(r) = \langle u, v \rangle,
\end{aligned}
\tag{4.108}
$$

which shows that $\mathscr{D}$ is unitary.

The dipole-sheet operator is closely related to a family of unitary operators in mD space discussed by LUDWIG [1966].

§ 5. Applications

5.1. EMISSION COMPUTED TOMOGRAPHY

Computed tomography, as introduced in § 2.1, uses a source of X-rays outside the patient's body to measure the transmission of X-rays along many straight-line paths through the body. This transmission, as shown by (2.3), is simply related to the line integral of the X-ray attenuation coefficient $\mu(r)$ along the line from the source to the detector. The goal of the procedure is to reconstruct a 2D map of the attenuation coefficient.

Emission computed tomography (ECT), on the other hand, is a nuclear-medicine procedure in which the source of radiation is *inside* the patient's body. A radioactive pharmaceutical which concentrates preferentially in certain organs is administered, and the goal of the procedure is to map the distribution of radioactivity in the body.

ECT comes in two flavors, SPECT and PET. In SPECT (single-photon emission computed tomography), the radioisotope emits a single gamma ray in each nuclear decay event. The most common isotope is ^{99m}Tc, for which the gamma-ray energy is 140 kV. PET (positron emission tomography) uses isotopes like ^{11}C, ^{13}N, ^{15}O, and ^{19}F that emit positrons (antielectrons) when they decay. The positrons lose their kinetic energy within a few millimeters of where they originate and are thus not detectable outside the body. However, the positrons are annihilated by interaction with electrons in the tissue, producing two high-energy (511 keV) gamma rays. These photons are detected in coincidence by external detectors, producing line-integral data from which the isotope distribution can be reconstructed.

Although the hardware for PET is varied and complicated, the reconstruction methods are rather straightforward implementations of the 2D inverse Radon transform. (CORMACK [1973] suggested the use of the 3D transform for PET, but to date no system using this principle has been built.) Therefore, PET offers no essential new insights into the mathematics and will not be discussed further here. For a review, see BROWNELL, CORREIA and ZAMENHOF [1978].

SPECT, on the other hand, is mathematically novel in two respects: (1) it can involve either the 2D or the 3D Radon transform; (2) the attenuation of the radiation in the body leads to a new transform, the *attenuated Radon transform*.

A simple system for acquiring projection data in nuclear medicine is shown in Fig. 6. A position-sensitive detector such as an Anger scintillation camera (ANGER [1958, 1964]) is placed behind a parallel-hole collimator – essentially a thick block of lead with many holes bored in it. A particular element of the detector receives radiation that passes through a single bore of the collimator. If scattered radiation is negligible, the radiation reaching this detector element must have originated in a thin pencil-like region of the object. Therefore, if the collimator bores are long and slender and if the attenuation of the radiation by the patient's body can be neglected (a point to which we shall return below),
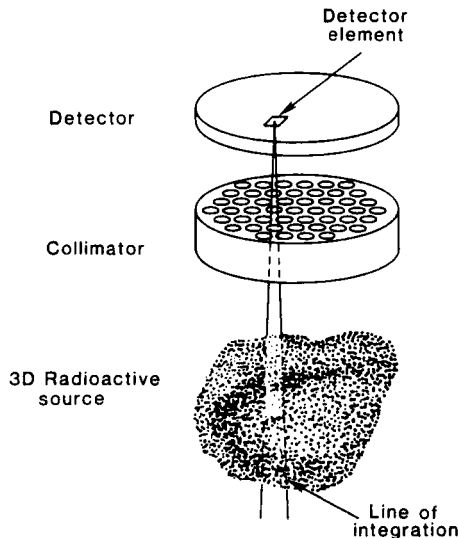

Fig. 6. A simple system for acquiring line-integral projection data in nuclear medicine. The detector is shown separated from the collimator for clarity, but in practice it would be in close proximity. Radiation reaching one detector element originates along a line in the object.

then the average flux at each detector element is, to a good approximation, proportional to a line integral of the isotope distribution. The entire 2D image for one position of the detector and collimator is thus a 2D line-integral projection of the 3D object; however, any one line of the 2D image is a 1D projection of a 2D slice of the object, which is just the usual CT projection, $\lambda_\phi(p)$ for fixed ϕ. To acquire the complete projection data set, the collimator and detector must be rotated around the object.

If a planar integral of the isotope distribution is desired, it can be obtained by integrating the 2D projection along lines. However, a more efficient way to get the same information is shown in Fig. 7. Here, an assembly of lead slats collimates the radiation in one direction only (KEYES [1975]). The 2D flux pattern on the detector varies in the direction perpendicular to the slats, but is constant parallel to them, at least on the average. The flux reaching one strip on the detector is, under the same assumptions as above, proportional to a planar integral of the isotope distribution. For one orientation of the collimator, the system measures $\lambda_{\hat{n}}(p)$ for fixed $\hat{n}$, where $\hat{n}$ is normal to the slats.

We saw in § 3.2 that $\hat{n}$ must explore a full hemisphere of directions to produce a complete 3D Radon transform. Thus the collimator and detector must be systematically scanned. For example, the slats could be rotated 180° about a normal to the detector face, then this normal could be incremented by some small angle, and the process repeated many times.
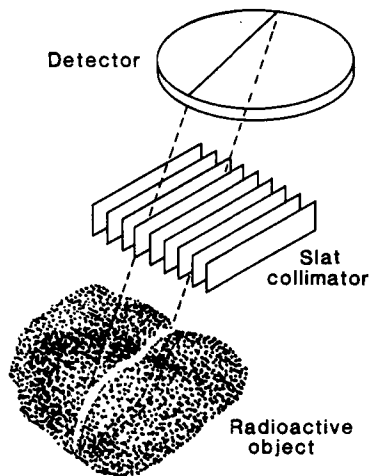

Fig. 7. System for acquiring planar-integral projection data in nuclear medicine. In practice, the detector would be in close proximity to the slat collimator. Radiation reaching a strip on the detector originates from a plane of the object.

A disadvantage of the slat collimator is that two scanning motions are required. The advantages are that the system efficiently collects photons and that the detector needs to have spatial resolution in only the direction perpendicular to the slats (GINDI, ARENDT, BARRETT, CHIU, ERVIN, GILES, KUJOORY, MILLER and SIMPSON [1982]). Furthermore planar integrals may be superior to line integrals when the data are noisy or incomplete. For example, RADULOVIC and VEST [1975] point out that good numerical reconstructions are still possible when $\hat{n}$ covers significantly less than 2π steradians.

In discussing the parallel-hole and slat collimators above, we neglected the attenuation of the radiation in the patient's body. In fact, this is a terrible approximation. The attenuation coefficient of soft tissue at 140 keV, for example, is about $0.15\,\text{cm}^{-1}$, so just 6 cm of tissue causes $1/e$ attenuation. What is measured with the parallel-hole collimator is not line integrals of the activity distribution, but exponentially weighted line integrals of the form

$$\lambda_\phi^{(e)}(p) = \int_\infty d^2r\, f(r)a(r; p, \phi)\delta(p - r\cdot\hat{n}), \qquad (5.1)$$

where $f(r)$ is the radioisotope distribution in a 2D object section, and the attenuation factor $a(r; p, \phi)$ is given by

$$a(r; p, \phi) = \exp\left[\int_r^D \mu(r')\,dl'\right], \qquad (5.2)$$

where the integral runs along a straight line from the source point r to the detector location D. Equation (5.1) is the attenuated Radon transform (GULLBERG [1979]). In general, $\lambda_\phi^{(e)}(p)$ depends on two arbitrary and independent 2D functions $f(r)$ and $\mu(r)$. There is a considerable literature on approximate and *ad hoc* inversions of (5.1). Good reviews are given by BUDINGER and GULLBERG [1977], GULLBERG [1979], and JASZCZAK, COLEMAN and LIM [1980].

A very important contribution to the theory of the attenuated Radon transform was recently made by TRETIAK and METZ [1980]. Their solution is exact when (1) the attenuation coefficient is independent of r, and (2) the body contours are convex and accurately known. Since these conditions are often satisfied to a good approximation, we shall give a detailed account of the TRETIAK–METZ algorithm.

The geometry is shown in Fig. 8. If μ is constant and the body is convex, (5.1) becomes

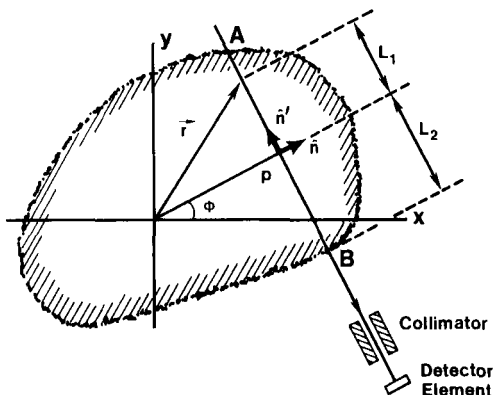$$\lambda_\phi^{(e)}(p) = \int_\infty d^2r\, f(r)\, e^{-\mu(L_1 + L_2)}\delta(p - r\cdot\hat{n}), \qquad (5.3)$$

Fig. 8. Geometry for the attenuated Radon transform.

where L_2 is a presumably known function of p, ϕ, and the body contours, and $L_1 = r \cdot \hat{n}'$, with $\hat{n}' \perp \hat{n}$.

In the Tretiak–Metz algorithm, a modified projection $\tilde{\lambda}_\phi(p)$ is formed by multiplying the original projection $\lambda_\phi^{(e)}(p)$ by the exponential factor $\exp(\mu L_2)$. The modified projection must be convolved with a 1D filter function $h(p)$ and then back-projected with another exponential weighting factor $\exp(\mu L_1)$. This algorithm differs from the standard inverse Radon transform (2.21) by the presence of the weighting factors and in the functional form of $h(p)$. The estimate $f(r)$ of the activity distribution is thus

$$f(r) = \int_0^{2\pi} d\phi \, \exp(\mu L_1)[\tilde{\lambda}_\phi(p) * h(p)]_{p=r\cdot\hat{n}}, \qquad (5.4)$$

where

$$\tilde{\lambda}_\phi(p) = \lambda_\phi^{(e)}(p) \exp(\mu L_2). \qquad (5.5)$$

Note that the integral runs over 2π radians; $\lambda_\phi^{(e)}$ and $\lambda_{\phi+\pi}^{(e)}$ are not redundant because of the attenuation factor.

The filter $h(p)$ is most easily described in the frequency domain; its 1D Fourier transform is

$$H(v) = \tfrac{1}{2}|v| \left[1 - \mathrm{rect}\left(\frac{\pi v}{\mu}\right) \right]. \qquad (5.6)$$

This function is illustrated in Fig. 9. It is the usual $|v|$ filter but with a gap in the interval $(-\mu/2\pi, \mu/2\pi)$.
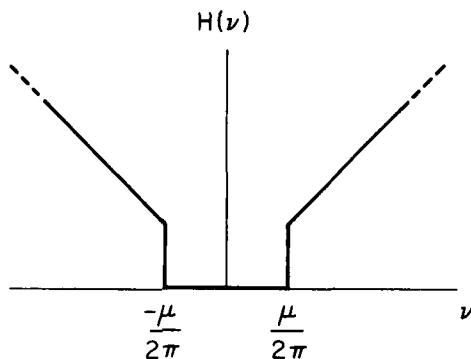
Fig. 9. Filter used in the TRETIAK–METZ algorithm.

To show that (5.4) and (5.5) constitute an exact inverse transform, let us consider a single point object at a general point r_0:

$$f^\delta(r) = \delta(r - r_0).\tag{5.7}$$

The attenuated Radon transform of this object is

$$\lambda_\phi^{(e,\delta)}(p) = e^{-\mu(L_{10} + L_2)}\delta(p - r_0 \cdot \hat{n}),\tag{5.8}$$

where

$$L_{10} = r_0 \cdot \hat{n}'.\tag{5.9}$$

Inserting (5.8) into (5.4) yields

$$\hat{f}^\delta(r) = \int_0^{2\pi} d\phi\, e^{\mu(r - r_0)\cdot\hat{n}'}\, h[(r - r_0) \cdot \hat{n}].\tag{5.10}$$

This equation gives the point spread function (PSF) of the system. The PSF depends only on the difference $r - r_0$, and the system is therefore shift-invariant. Since the integral runs over 2π, we can choose the axes so that $r - r_0$ is along the x-axis. Then

$$\hat{f}^\delta(r) = \int_0^{2\pi} d\phi\, e^{\mu R \sin\phi} h(R \cos \phi),\tag{5.11}$$

where $R = |r - r_0|$. If we represent $h(R \cos \phi)$ in terms of its Fourier transform, (5.11) becomes

$$\hat{f}^\delta(r) = \int_0^{2\pi} d\phi\, e^{\mu R \sin\phi} \int_{-\infty}^{\infty} H(\nu)\, e^{2\pi i \nu R \cos \phi}\, d\nu.\tag{5.12}$$

The integral over ϕ is (GRADSHTEYN and RYZHIK [1980] p. 488; TRETIAK and METZ [1980]),

$$\int_0^{2\pi} e^{\mu R \sin \phi} e^{2\pi i \nu R \cos \phi} \, \mathrm{d}\phi = 2\pi J_0\{R[(2\pi\nu)^2 - \mu^2]^{1/2}\}, \qquad (2\pi\nu)^2 > \mu^2.$$

(5.13)

With (5.6), (5.13) and a change of variables, (5.12) becomes

$$\hat{f}^\delta(r) = 2\pi \int_{\mu/2\pi}^\infty \nu \, \mathrm{d}\nu \, J_0\{R[(2\pi\nu)^2 - \mu^2]^{1/2}\} = 2\pi \int_0^\infty \rho \, \mathrm{d}\rho \, J_0(2\pi\rho R),$$

(5.14)

where

$$\rho^2 = \nu^2 - (\mu/2\pi)^2.$$

(5.15)

We recognize (5.14) as the Hankel transform of unity. Since the Hankel transform is the 2D Fourier transform for rotationally symmetric functions, we have

$$f^\delta(r) = \delta(r - r_0),$$

(5.16)

which is an exact reconstruction of the original $f^\delta(r)$. Since this result was obtained for an arbitrary r_0, it holds for any object by linear superposition, and the TRETIAK–METZ formula is an exact inverse to the attenuated Radon transform with constant attenuation (CLOUGH and BARRETT. [1983]). In practice, some apodized approximation to $H(\nu)$ would be used, just as in the unattenuated case, but with the form (5.6), the inverse is mathematically exact.

It may seem surprising that an exact reconstruction can be obtained with a finite gap in the frequency space. This is possible because the central-slice theorem does not hold in the attenuated case. A frequency component ν in the projection does not correspond uniquely to a frequency $\rho = \hat{n}\nu$ in the object, and no object frequencies are irretrievably lost by the gap in $H(\nu)$.

Although many important properties of the attenuated Radon transform have been given by GULLBERG [1979], BELLINI, PIACENTINI, CAFFORIO and ROCCA [1979], and TRETIAK and DELANEY [1977], further work is still needed to generalize the TRETIAK–METZ theory to non-convex objects and inhomogeneous μ, and also to the 3D case.

A related transform, the attenuated Abel transform, was recently derived by CLOUGH and BARRETT [1983].

5.2. NMR IMAGING

   Nuclear magnetic resonance (NMR) has long been an important research tool in physics and chemistry. It occurs because any nucleus with an unpaired proton or neutron possesses an intrinsic magnetic moment μ and a spin angular momentum $\hbar I$. These two quantities are related by

$$\mu = \gamma \hbar I, \tag{5.17}$$

where the constant γ is called the magnetogyric ratio. In a static magnetic field B_0, the interaction energy of the nuclear magnetic dipole is

$$U = -\mu \cdot B_0. \tag{5.18}$$

For a nucleus with nuclear spin $I = \frac{1}{2}$ such as hydrogen, the component of μ parallel to B_0 can be only $\pm \frac{1}{2}\gamma\hbar$, and the energy difference between these two quantum states is

$$\Delta U = \gamma \hbar B_0. \tag{5.19}$$

If a radio-frequency (RF) magnetic field of frequency ω is applied, it can induce transitions between the energy levels provided

$$\hbar \omega = \Delta U \tag{5.20a}$$

or

$$\omega = \gamma B_0. \tag{5.20b}$$

This condition for resonant absorption is called the Larmor condition, and γB_0 is the Larmor frequency ω_L. For hydrogen, $\gamma = 2.675 \times 10^8 \, s^{-1} \, \text{tesla}^{-1}$, and

$$\nu_L (\text{MHz}) = 42.58 B_0 \text{ (tesla)}, \tag{5.21}$$

where $\nu_L = \omega_L / 2\pi$ and 1 tesla = 10^4 gauss.
   NMR experiments involve a large number N of nuclei, N_+ of which are in the upper state and N_- in the lower state. In thermal equilibrium,

$$\frac{N_+}{N_-} = \exp[-\gamma \hbar B_0 / k_B T] \approx 1 - \gamma \hbar B_0 / k_B T, \tag{5.22}$$

where k_B is Boltzmann's constant and T is the absolute temperature. For example, if $T = 300\,^\circ K$ and $B_0 = 0.1$ tesla, then $N_+ / N_- = 1 - (6.7 \times 10^{-7})$. Thus, the populations are very nearly equal, and absorption and stimulated emission are almost equally probable, but the entire resonant effect comes from the small difference in population.

It is often convenient to consider the net macroscopic magnetization M rather than the magnetic moment of individual nuclei. Since magnetization is magnetic moment per unit volume, we have

$$M = \frac{1}{V} \sum_{i=1}^{N} \mu_i \qquad (5.23)$$

where μ_i is the moment of the ith nucleus and V is the volume in which the N nuclei are contained. Because of the near balance between the two possible orientations of each μ_i, $|M|$ is much less than $N\mu/V$. For most purposes, M may be treated as a classical vector.

A magnetic dipole μ in a field B_0 experiences a torque $\mu \times B_0$. The torque is the rate of change of the angular momentum, which in turn is connected to μ by (5.17). Combining this result with (5.23) shows that

$$\frac{dM}{dt} = \gamma M \times B_0. \qquad (5.24)$$

Thus, if M is initially not parallel to B_0, its time derivative will be perpendicular to both M and B_0; in other words, M precesses about B_0 like a gyroscope. (See Fig. 10.) Equation (5.24) would be correct if no other forces besides that due to B_0 acted on M. In fact, we must consider three other effects: (1) the RF field; (2) longitudinal relaxation; (3) transverse relaxation.

The RF field may be accounted for by adding B_{RF} to B_0 in (5.24). However, B_{RF} is usually applied in short pulses, and the total field is just B_0 between pulses.

Longitudinal relaxation occurs because the spin system can exchange energy with its environment or "lattice", for example by emitting or absorbing phonons. This relaxation, which tends to reduce the angle between M and B_0, may be

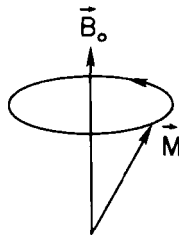

Fig. 10. The magnetization vector M precesses with angular velocity ω_L in a static magnetic field B_0.

described phenomenologically by

$$\frac{dM_z}{dt} = \frac{M_0 - M_z}{T_1},$$ (5.25)

where it is assumed that B_0 is parallel to the z-axis, M_0 is the thermal-equilibrium value of M_z, and T_1 is called the spin-lattice or longitudinal relaxation time.

Relaxation of the transverse components of M occurs by spin-lattice interaction and also because the local magnetic field is not identical at each nucleus. In addition to B_0 and B_{RF}, there is a field on a particular nucleus due to the magnetic moments of all other nuclei. This fluctuating field alters the precession frequency and broadens the absorption line. Because of the difference in precession frequency, the spins tend to "dephase" and the transverse components μ_x and μ_y are randomized after a characteristic time T_2. That means that the net transverse components of the magnetization, M_x and M_y, relax to zero with this time constant T_2, usually called the spin-spin or transverse relaxation time.

Accounting for all of these effects, we obtain the Bloch equations,

$$\frac{dM_z}{dt} = \gamma(M \times B)_z + \frac{M_0 - M_z}{T_1},$$ (5.26)

$$\frac{dM_x}{dt} = \gamma(M \times B)_x - \frac{M_x}{T_2},$$ (5.27)

$$\frac{dM_y}{dt} = \gamma(M \times B)_y - \frac{M_y}{T_2},$$ (5.28)

where $B = B_0 + B_{RF}$.

When the spin system absorbs energy from the RF pulse, the magnetization is tipped away from the z-axis and begins to precess. This creates transverse components of M oscillating at frequency ω_L and decaying with time constant T_2. A set of receiver coils can then pick up a signal, called the free-induction decay signal, from which one can deduce the spin density and T_2.

Many other ingenious schemes have been developed to measure the spin density N/V, magnetogyric ratio γ, and relaxation times T_1 and T_2. For a review, see ABRAGAM [1961], FARRAR and BECKER [1971], or SLICHTER [1963]. However, in all of these methods, it is assumed that the quantity being measured is homogeneously distributed throughout the specimen, and great care is exercised to make the applied field homogeneous as well. Thus the measure-

ment involves a volume integral of some quantity over the volume of the specimen. More recently, great progress has been made in extracting information about the *spatial* distribution of spin density and relaxation time. These efforts have given rise to the new and exciting field of *NMR imaging* or *zeugmatography* (from the Greek ζευγμα, "that which joins together"). Recent reviews of this field, emphasizing clinical applications, have been given by PYKETT [1982], PYKETT, NEWHOUSE, BUONANNO, BRADY, GOLDMAN, KISTLER and POHOST [1982], MANSFIELD and MORRIS [1982], KAUFMANN, CROOKS and MARGULIS [1981], and KARSTAEDT, WITCOFSKI and PARTAIN [1981].

Since the human body is mainly water, almost all medical imaging applications of NMR have used the resonance of the proton or hydrogen nucleus. (^{16}O does not have a nuclear magnetic moment since it contains an even number of protons and neutrons.) The imaging instruments that are being developed thus have as their goal the mapping of proton density $n(r)$ (essentially, water density) or proton relaxation times $T_1(r)$ or $T_2(r)$. Either true 3D maps or a series of 2D slices can be produced, and all of the instruments have the capability of producing images that emphasize $n(r)$, $T_1(r)$, or $T_2(r)$ as desired, simply by using different RF pulse sequences.

NMR imaging systems are often classified as point, line, plane, or volume systems. Point systems collect data from a small, isolated region of the object at a time; 2D or 3D information is built up by scanning the sensitive point over the object. This procedure is straightforward but inefficient, and all modern systems collect data from a larger region simultaneously. They all, in one guise or another, measure either a 2D or a 3D Radon transform.

Let us consider first a few of the many ways to isolate a single plane. For this purpose, the magnetic field must be inhomogenous, since otherwise all points in the volume would be equivalent and no spatial resolution would be possible. The usual approach is to add a weak "gradient field" that varies linearly with position. More precisely, if the large static field B_0 is in the z direction, the z component of the total field is

$$B_z = B_0 + \alpha(r \cdot \hat{n}), \tag{5.29}$$

where $\nabla B_z = \alpha \hat{n}$ with α constant. The x and y components of the gradient field do not influence the resonant frequency in first order since

$$B = [B_x^2 + B_y^2 + B_z^2]^{1/2} \approx B_z + \frac{B_x^2 + B_y^2}{2B_z^2}, \tag{5.30}$$

which is negligibly different from B_z if B_x, $B_y \ll B_0$.

Now suppose that the nuclear spin system is excited with a relatively long RF pulse having a well-defined frequency ω_0. Only the spins with $\omega_L = \omega_0$ will resonantly absorb energy, and only these will contribute to the NMR signal. From (5.20) and (5.29), the resonant spins lie on the plane defined by

$$\omega_0 - \gamma B_0 = \alpha\gamma(r \cdot \hat{n}), \tag{5.31}$$

and the signal yields one point in a 3D Radon transform. The quantity being transformed depends in a complicated way on the RF pulse sequence and subsequent signal processing; in general, it is some mixture of $n(r)$, $T_1(r)$, and $T_2(r)$.

The method just described yields one planar integral in a single measurement, and a time of about $3T_1$ must be allowed for the system to return to equilibrium before another measurement can be made. Since several hundred measurements must be made to adequately sample the 3D Radon space, and T_1 is typically $0.1-1$ s, the imaging time with this method is rather long. However, a slight modification of the method allows the simultaneous measurement of integrals on a set of parallel planes. If the RF pulse is very short so that it contains a broad spectrum of frequencies, all spins in the volume are simultaneously excited. Alternatively, if the gradient field is applied *after* excitation, all spins will have the same resonant frequency when they are excited. In either case, the precession frequency depends on the local field during precession, not during excitation. Therefore, each plane of constant field will contain spins precessing at a characteristic frequency and with a transverse component of M decaying with time constant T_2. The overall NMR signal will be a superposition of these free-induction decay signals (Fig. 11). A Fourier analysis serves to separate the composite signal into its individual frequencies, each frequency corresponding to one plane in the object. This procedure yields points along a line in 3D Radon space, and the direction of the field gradient $\hat{n}$ can be varied on subsequent excitations to sample the full Radon volume. Reconstruction of the full 3D image of the object can then be carried out by any of the methods discussed in § 3 (SHEPP [1980]; MARR, CHEN and LAUTERBUR [1981]).

If only one or a few planes of the object are to be imaged, it is simpler to use line integrals and the 2D Radon transform. One way to accomplish this is to use two orthogonal field gradients, say one in the z direction and one in the $x-y$ plane. Originally, only the z gradient is applied and a narrow-band RF pulse is used to selectively excite spins in a plane normal to the z-axis. Then the z gradient is switched off, the $x-y$ gradient is turned on, and the free induction decay is observed. If this gradient is in direction $\hat{n}$ in the $x-y$ plane, all spins in a plane perpendicular to $\hat{n}$ would have the same precession
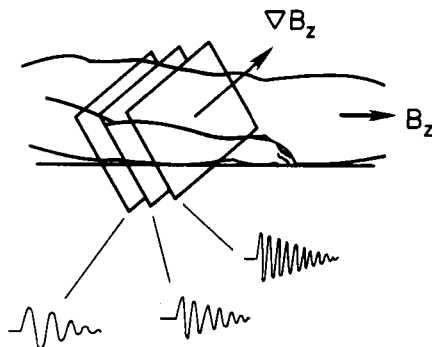
Fig. 11. Illustration of one way to acquire planar-integral data in NMR imaging. All spins in a volume are simultaneously excited. When they decay in a field gradient, each plane has a characteristic frequency, and the planes can be separated by a Fourier transform of the received signal.

frequency, but not all of these spins were excited. The signal at a particular frequency thus comes from spins along the line defined by the intersection of the plane of excitation and a plane normal to $\hat{n}$. The complete Fourier transform of the free-induction decay signal is thus equivalent to a 1D projection of the 2D slice selected during excitation. In subsequent excitations, the direction $\hat{n}$ is varied, and a full 2D Radon transform is sampled. Any variations of the 2D inverse Radon transform can be used for reconstruction.

5.3. ELECTROSTATICS

There is a close connection between Radon theory and electrostatics, as might be expected by the occurrence of the Laplacian operator ∇^2 in the inverse Radon transform. Indeed, Radon himself was motivated by this connection to consider the problem in the first place, and he originally found the inverse transform by using known results of potential theory.

Electrostatics is based on Poisson's equation,

$$\nabla^2 \Phi(r) = -4\pi\rho(r), \tag{5.32}$$

where $\Phi(r)$ is the electrostatic potential and $\rho(r)$ is the charge density. If there are no boundaries and $\rho(r)$ is known for all r, the solution of Poisson's equation in 3D is well known to be

$$\Phi(r) = -4\pi\nabla^{-2}\rho(r) = \int_\infty d^3r' \, \frac{\rho(r')}{|r - r'|}, \tag{5.33}$$

where ∇^{-2} is the inverse of the Laplacian operator ∇^2. Comparing this result to (3.16), we see that $\Phi(r)$ is the summation image of $\rho(r)$, obtained by taking the 3D Radon transform, back-projecting, and summing over all projection directions in 2π steradians. In operator form (RADON [1917]),

$$\Phi = \frac{1}{\pi} \mathcal{B}_3 \mathcal{R}_3 \rho. \tag{5.34}$$

This is consistent with Poisson's equation since, by (3.26),

$$\mathcal{R}_3^{-1} = -\frac{1}{4\pi^2} \nabla^2 \mathcal{B}_3. \tag{5.35}$$

Therefore, we may formally write the inverse Laplacian as

$$\nabla^{-2} = -\frac{1}{4\pi^2} \mathcal{B}_3 \mathcal{R}_3. \tag{5.36}$$

We may verify that this result is consistent with (5.33) by writing the operators out in detail. This gives

$$\Phi(r) = \frac{1}{\pi} \int_{2\pi} d\Omega_n \left[\int_\infty d^3r' \, \rho(r')\delta(p - r' \cdot \hat{n}) \right]_{p = r \cdot \hat{n}}$$

$$= \frac{1}{\pi} \int_\infty d^3r' \, \rho(r') \int_{2\pi} d\Omega_n \, \delta[(r - r') \cdot \hat{n})]$$

$$= \int_\infty d^3r' \, \frac{\rho(r')}{|r - r'|}, \tag{5.37}$$

where the last step follows from (3.15). Thus, the operator form (5.36) is indeed equivalent to (5.33). The function $|r - r'|^{-1}$ plays the dual role of point spread function in the summation image and Green's function for Poisson's equation.

In 2D, the situation is a little more complicated. Poisson's equation has the same form,

$$\nabla^2\Phi(r) = -4\pi\rho(r); \qquad \Phi(r) = -4\pi\nabla^{-2}\rho(r), \tag{5.38}$$

but we know from (2.56) that

$$\nabla^{-2} = \frac{1}{2\pi^2} \mathcal{B}_2[\ln|p| *]\mathcal{R}_2. \tag{5.39}$$

Writing the operators out in detail, we find

$$\Phi(r) = -\frac{2}{\pi} \int_0^\pi d\phi \int_{-\infty}^\infty dp \ln|p - r \cdot \hat{n}| \int_\infty d^2r' \, \rho(r')\delta(p - r' \cdot \hat{n})$$

$$= -\frac{2}{\pi} \int_0^\pi d\phi \int_\infty d^2r' \, \rho(r') \ln|(r' - r) \cdot \hat{n}|. \qquad (5.40)$$

The ϕ integral is given by

$$\int_0^\pi d\phi \ln[\,|r - r'| \cdot \cos\psi|\,] = \pi \ln[\,|r - r'|\,] + \tfrac{1}{2} \int_0^{2\pi} d\psi \ln[\,|\cos\psi|\,], \qquad (5.41)$$

where ψ is the angle between $r - r'$ and $\hat{n}$. The integral over ψ is just some constant C, independent of r and r', and (5.40) becomes

$$\Phi(r) = -2 \int_\infty d^2r' \, \rho(r')\{\ln|r - r'| + C\}. \qquad (5.42)$$

The value of C is irrelevant since an additive constant in the potential does not influence the electric field.

To show that (5.42) is indeed a solution of (5.38), we can operate on it with ∇^2 and recognize that (MORSE and FESHBACH [1953] p. 891)

$$\nabla^2 \ln|r - r'| = 2\pi\delta(r - r'). \qquad (5.43)$$

and, of course, $\nabla^2 C = 0$.

In 2D, the Green's function for Poisson's equation is *not* the same as the PSF in the summation image; the former is $-2\ln|r - r'|$ and the latter is $|r - r'|^{-1}$.

5.4. WAVE PROPAGATION

Before the advent of CT, the prime motivation for study of the Radon transform was its usefulness in radiation and scattering problems (JOHN [1955]; COURANT and HILBERT [1962]; LAX and PHILLIPS [1967]). These problems usually involve solution of the time-dependent homogeneous scalar wave equation,

$$\left(\nabla^2 - \frac{1}{c^2}\frac{\partial^2}{\partial t^2}\right)\psi(r, t) = 0. \qquad (5.44)$$

There is an intimate connection between the wave equation and the Radon transform because the general solution of the wave equation can be written as a superposition of plane waves. This statement is a commonplace if we think in terms of *harmonic* plane waves of the form $\exp(i\mathbf{k}\cdot\mathbf{r} - i\omega t)$, but the term plane waves has a much broader meaning than that. It refers to any function that is constant on a plane. Since $\mathbf{r}\cdot\hat{n}$ is constant on any plane normal to $\hat{n}$, we can construct plane waves at will by making functions of $\mathbf{r}\cdot\hat{n}$. Examples of mathematical interest (JOHN [1955]; COURANT and HILBERT [1962]) include power-law plane waves $|p - \mathbf{r}\cdot\hat{n}|^k$, logarithmic plane waves $\ln|p - \mathbf{r}\cdot\hat{n}|$, and impulsive plane waves $\delta(p - \mathbf{r}\cdot\hat{n})$ or $\delta'(p - \mathbf{r}\cdot\hat{n})$. The latter, of course, form the basis functions for the Radon and dipole-sheet transforms, respectively. To make any of these functions into solutions of the homogeneous wave equation, we need only choose $p = \text{constant} + ct$. For example, from (4.98), it is readily seen that

$$\left(\nabla^2 - \frac{1}{c^2}\frac{\partial^2}{\partial t^2}\right)\delta(p_0 + ct - \mathbf{r}\cdot\hat{n}) = 0. \tag{5.45}$$

This function represents a planar sheet moving with velocity c in the direction $\hat{n}$ and at a perpendicular distance p_0 from the origin at $t = 0$.

To see the usefulness of plane-wave decompositions, let us use the tools assembled in §§ 3 and 4 to solve *Cauchy's problem*, in which we wish to find the solution to (5.44) subject to the initial conditions

$$\psi(\mathbf{r}, 0) = 0, \qquad \left.\frac{\partial\psi(\mathbf{r}, t)}{\partial t}\right|_{t=0} = v(\mathbf{r}). \tag{5.46}$$

There are no sources present and no spatial boundaries except at infinity. Once we have solved this problem, the more general solution where $\psi(\mathbf{r}, 0) \neq 0$ can be readily deduced (COURANT and HILBERT [1962] p. 682).

The general procedure is quite analogous to a Fourier decomposition. We write the solution as a superposition of plane waves with initially unknown expansion coefficients, then choose these coefficients to satisfy the initial conditions. Using impulsive plane waves as the basis, we can write

$$\psi(\mathbf{r}, t) = \int_{2\pi} d\Omega_n \int_{-\infty}^{\infty} dp\, g(p, \hat{n})\delta(p + ct - \mathbf{r}\cdot\hat{n}). \tag{5.47}$$

By differentiating under the integral sign, it is readily seen that this $\psi(\mathbf{r}, t)$ indeed satisfies the wave equation. To match the initial conditions, we must have

$$v(\mathbf{r}) = c\int_{2\pi} d\Omega_n \int_{-\infty}^{\infty} dp\, g(p, \hat{n})\delta'(p - \mathbf{r}\cdot\hat{n}). \tag{5.48}$$

From (4.83), we recognize the integral as an inverse dipole-sheet transform, so that

$$v(r) = 2\pi ic \, \mathscr{D}^{-1}\{g(p, \hat{n})/p\}. \tag{5.49}$$

Solving for $g(p, \hat{n})$, we find

$$g(p, \hat{n}) = \frac{p}{2\pi ic} \, \mathscr{D}\{v(r)\} = \frac{1}{4\pi^2 c} \int_\infty d^3 r' \, v(r') \, \delta'(p - r' \cdot \hat{n}). \tag{5.50}$$

Inserting (5.50) into (5.47) yields

$$\psi(r, t) = \frac{1}{4\pi^2 c} \int_{2\pi} d\Omega_n \int_{-\infty}^{\infty} dp \, \delta(p + ct - r \cdot \hat{n}) \int_\infty d^3 r' \, v(r') \delta'(p - r' \cdot \hat{n})$$

$$= \frac{-1}{4\pi^2 c} \int_{2\pi} d\Omega_n \int_\infty d^3 r' \, v(r') \delta'[ct - (r - r') \cdot \hat{n}]. \tag{5.51}$$

To put this result in a more familiar form, we can use (4.95) to write

$$\int_{2\pi} d\Omega_n \, \delta'[ct - (r - r') \cdot \hat{n}] = \frac{-\pi}{R} \delta(ct - R), \tag{5.52}$$

for $t > 0$ with $R = |r - r'|$. Then (5.51) reduces to the well-known solution (MORSE and FESHBACH [1953] p. 837)

$$\psi(r, t) = \frac{1}{4\pi c^2} \int_\infty d^3 r' \, v(r') \frac{1}{R} \delta\left(t - \frac{R}{c}\right). \tag{5.53}$$

An alternative solution can be obtained through the change of variables $R = r' - r$, so that

$$\psi(r, t) = \frac{1}{4\pi c^2} \int_{4\pi} d\Omega_R \int_0^{\infty} R \, dR \, v(r + R) \delta\left(t - \frac{R}{c}\right)$$

$$= \frac{t}{4\pi} \int_{4\pi} d\Omega_R \, v(r + ct\hat{R}), \tag{5.54}$$

where $t > 0$ and $\hat{R} = R/R$. Equation (5.54), which is known as *Poisson's solution* (MORSE and FESHBACH [1953] p. 847), makes it clear that $\psi(r, 0) = 0$, even though we did not explicitly use this condition.

The physical content of both (5.53) and (5.54) is the same: only points a distance ct away from the point r' are influenced by the initial conditions at

that point at $t = 0$. Equation (5.54) shows clearly that $\psi(r, t)$ is just the average of $v(r)$ over a sphere of radius ct about r. It is a *spherical mean* (JOHN [1955]).

It is worth dwelling for a moment on (5.52), where we converted a plane wave to a spherical wave by averaging over directions. The average of all dipole sheets a distance ct from a point is a spherical shell at that distance. The shell is, of course, the Green's function for the wave equation, which satisfies

$$\left(\nabla^2 - \frac{1}{c^2}\frac{\partial^2}{\partial t^2}\right)\frac{1}{R}\,\delta\left(t - \frac{R}{c}\right) = -4\pi\delta(t)\delta(\mathbf{R}). \tag{5.55}$$

The statement that an average plane wave is a spherical wave holds also for harmonic waves, since

$$\int_{4\pi} d\Omega_k\, e^{i(\mathbf{k}\cdot\mathbf{r} - \omega t)} = \frac{2\pi e^{-i\omega t}}{ik}\left[\frac{e^{ikr}}{r} - \frac{e^{-ikr}}{r}\right]$$

$$= 4\pi e^{-i\omega t}\frac{\sin kr}{kr}. \tag{5.56}$$

Once again we recognize a Green's function. this time for the Helmholtz equation:

$$(\nabla^2 + k^2)\frac{e^{\pm ikr}}{r} = -4\pi\delta(\mathbf{r}). \tag{5.57}$$

Equation (5.56) contains both incoming and outgoing spherical waves, so it is not a causal Green's function.

5.5. MICROWAVE SCATTERING

Following the lead of LAX and PHILLIPS, whose extensive work is detailed in their monograph (LAX and PHILLIPS [1967]), many theorists have applied the Radon transform to scattering studies, especially in the time domain. This topic is of great current interest because of its use in analyzing the "signature" of radar scatterers (KENNAUGH and MOFFATT [1965]; LEWIS [1969]; YOUNG [1976]; DAS and BOERNER [1978]; MAGER and BLEISTEIN [1978]; BOJARSKI [1979]; BOERNER [1979]; DEVANEY [1980]), and in microwave imaging (CHAN and FARHAT [1981]; ROCKMORE, DENTON and FRIED-LANDER [1979]). We shall indicate the general nature of the problem by calculating the temporal impulse response of a weak volume scatterer in the

Born approximation, but very similar results are obtained for metallic reflectors in the above references.

Consider a medium such as a tenuous vapor where the refractive index has the form

$$n(r) = 1 + \Delta n(r), \tag{5.58}$$

with $\Delta n(r) \ll 1$. We assume also that the medium is nondispersive so that Δn does not depend on wavelength. The velocity of an electromagnetic wave is then a function of position, denoted $c_m(r)$, and given by

$$c_m(r) = \frac{c}{1 + \Delta n(r)}, \tag{5.59}$$

and the scalar wave equation is

$$\left(\nabla^2 - \frac{1}{c_m^2} \frac{\partial^2}{\partial t^2} \right) \psi(r, t) = 0 \tag{5.60}$$

or, approximately,

$$\left(\nabla^2 - \frac{1}{c^2} \frac{\partial^2}{\partial t^2} \right) \psi(r, t) \approx \frac{2\Delta n(r)}{c^2} \frac{\partial^2 \psi(r, t)}{\partial t^2}. \tag{5.61}$$

The first Born approximation consists of replacing $\psi(r, t)$ on the right-hand side of this equation with the unperturbed incident wave $\psi_i(r, t)$. The wave equation is then inhomogeneous with a known source term, and the Green's-function solution is

$$\psi_s(r, t) = -\frac{1}{2\pi c^2} \int_{-\infty}^{t} dt' \int_{\infty} d^3r' \, \Delta n(r') \frac{\partial^2 \psi_i(r', t')}{\partial t'^2} \frac{\delta(\tau - R/c)}{R}, \tag{5.62}$$

where $\tau = t - t'$, $R = |r - r'|$, and the total wave $\psi(r, t) = \psi_i(r, t) + \psi_s(r, t)$.

Now we consider a point source located at $r = r_s$ and a point detector at $r = r_D$ as shown in Fig. 12. We shall regard the system of source, scatterer, and detector as a temporal filter and calculate its temporal impulse response $h(t)$, which depends on r_s, r_D, and $\Delta n(r)$. Thus, we assume that the source emits a very short pulse of radiation at $t = t_0$, so that the incident wave is

$$\psi_i(r', t') = \frac{1}{R_s} \delta \left(t' - t_0 - \frac{R_s}{c} \right), \tag{5.63}$$

Source

Detector

r_s

Scattering
element

r_D

Scattering
element

r'

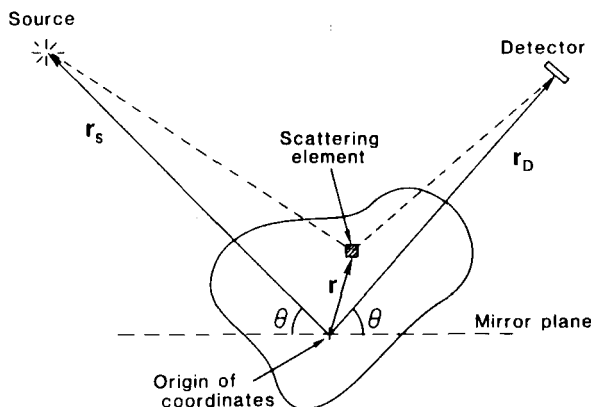θ θ Mirror plane

Origin of
coordinates

Fig. 12. Geometry for calculation of the temporal impulse response of a weak volume scatterer. If r_S and r_D are large, all points on the "mirror plane" or any plane parallel to it give approximately the same time delay for waves propagating from source to scattering point to detector, and the received signal at one time τ is proportional to the integral of $\Delta n(r)$ over this plane.

where $R_s = |r' - r_s|$. The impulse response $h(t)$ is the wave at the detector at time t, given from (5.62) and (5.63) by

$$h(t) = -\frac{1}{2\pi c^2} \int_{-\infty}^{t} dt' \int_{\infty} d^3 r' \frac{\Delta n(r')}{R_s R_D} \delta'' \left(t' - t_0 - \frac{R_s}{c} \right) \delta \left(t - t' - \frac{R_D}{c} \right),$$

(5.64)

where $R_D = |r' - r_D|$.

We next make the Fraunhofer approximation, valid for r_s and r_D large compared to the size of $\Delta n(r')$, so that

$$R_s = r_s - \hat{r}_s \cdot r' + \ldots, \qquad (5.65)$$

$$R_D = r_D - \hat{r}_D \cdot r' + \ldots, \qquad (5.66)$$

where $r_s = |r_s|$, $\hat{r}_s = r_s/r_s$, and similarly for r_D. We retain only the first term in each expansion in the denominator of (5.64), but the first two terms in the arguments of the delta functions. This yields

$$h(t) = -\frac{c}{2\pi r_D r_s} \int_{\infty} d^3 r' \, \Delta n(r') \delta''(p - r' \cdot \hat{n}) \qquad (5.67)$$

where

$$p = -c(t - t_0) + r_s + r_D, \qquad (5.68)$$

$$\hat{n} = \hat{r}_s + \hat{r}_D. \qquad (5.69)$$

Neglecting a distortion that arises because $\hat{n}$ is not really a unit vector, we can write

$$h(t) = \text{const.} \cdot \left[\frac{\partial^2}{\partial p^2} \mathcal{R}_3\{\Delta n(r)\} \right]. \tag{5.70}$$

This result has a simple physical interpretation. All points r' that have the same propagation delay (from source to scattering point to detector) contribute to $h(t)$ for the same t. (See Fig. 12.) If r_s and r_D are large, these points lie on a surface that is approximately planar and normal to $\hat{r}_s + \hat{r}_D$. One can think of points on this plane forming a mirror. The occurrence of $\partial^2/\partial p^2$ in (5.70) is also understandable. If $\Delta n(r)$ is either invariant or linearly varying in the direction $\hat{n}$, there is no reflection from this "mirror".

Another way to understand (5.70) is to take its temporal Fourier transform, yielding the standard Born-approximation result (WOLF [1969]; DÄNDLIKER and WEISS [1970])

$$H(v) = \text{const.} \, v^2 \int_\infty \mathrm{d}^3 r' \, \Delta n(r') \exp\left[(2\pi i v/c)(\hat{n} \cdot r')\right]. \tag{5.71}$$

The factor v^2 corresponds to the second derivative, and the integral is recognized as a 3D *spatial* Fourier transform, with spatial frequency

$$\sigma = v\hat{n}/c.$$

Thus, a monochromatic source of frequency v at r_s and a detector at r_D give information about one point in the 3D Fourier transform of $\Delta n(r)$. Varying v, but keeping r_s and r_D fixed, gives information about other spatial frequencies along a line in direction $\hat{n}$ in Fourier space. The temporal impulse contains all temporal frequencies, and hence maps out this entire line in one measurement. By the central-slice theorem, this information is equivalent to $\lambda_{\hat{n}}(p)$ for all p and fixed $\hat{n}$.

Very similar results have been obtained by LACOURT, VIENOT and GOEDGEBUER [1976] for the temporal impulse response of a 2D diffracting aperture.

5.6. COMPTON SCATTERING

The inelastic scattering of X-rays by electrons was first discovered by FLORANCE [1910] and GRAY [1913]. However, the effect is now associated

with the name of A. H. COMPTON [1923a,b; 1926], who carried out a series of very precise experiments and gave a theoretical explanation of the main features of the observations. A good account of the early history is given by STUEWER and COOPER [1977].

An elementary derivation of the energy loss by Compton scattering considers the electron to be free and initially at rest (see, for example, TIPLER [1969]). The incident X-ray photon has energy E_0. After scattering through an angle θ, it has a reduced energy E, given by

$$\frac{1}{E} = \frac{1}{E_0} + \frac{1}{mc^2}(1 - \cos\theta), \qquad (5.72)$$

with m being the rest mass of the electron and c being the speed of light. The important point for the present discussion is that there is a unique relationship between E and θ; the photons scattered through one particular angle θ have a discrete energy E.

The situation is very different when the electrons are initially not at rest but have some distribution of momenta, as they must when they are bound to an atom. Then the scattered photons, even for fixed θ, have a distribution of energies, and analysis of this energy spectrum can give information about the momentum distribution of the scattering electrons. This information is of fundamental importance because the probability density function for the electron momentum P is given by

$$n(P) = \chi^*(P)\chi(P), \qquad (5.73)$$

where $\chi(P)$ is the electron wavefunction in the momentum representation, which is just the 3D Fourier transform of the usual configuration-space wavefunction $\psi(r)$. Thus, measurement of the Compton spectrum provides a direct check on theoretical wavefunctions (WILLIAMS [1977]).

A simple classical analysis that shows the relationship between $n(P)$ and the Compton spectrum was given by DuMOND [1929, 1933]. See also STUEWER and COOPER [1977] and PLATZMAN and TZOAR [1977]. The analysis is just a nonrelativistic application of the principles of conservation of energy and momentum. The photon momentum before scattering is $\hbar k_0$, where k_0 is the wavevector. The momentum after scattering is $\hbar k$. The photon energy before and after scattering is $\hbar c k_0$ and $\hbar c k$, respectively. The electron momentum after scattering is $P + \Delta P$, where, by conservation of momentum,

$$\Delta P = \hbar(k - k_0) \equiv -\hbar\Delta k. \qquad (5.74)$$

The energy gained by the electron, and hence, lost by the photon, is

$$\Delta E = E_0 - E = \frac{|P + \Delta P|^2}{2m} - \frac{P^2}{2m} = \frac{|\Delta P|^2}{2m} + \frac{P \cdot \Delta P}{m}$$

$$= \frac{\hbar^2}{2m}(k^2 + k_0^2 - 2k \cdot k_0) - \frac{\hbar}{m} P \cdot \Delta k$$

$$= \frac{E^2}{2mc^2} + \frac{E_0^2}{2mc^2} - \frac{EE_0}{mc^2}\cos\theta - \frac{\hbar}{m} P \cdot \Delta k. \qquad (5.75)$$

This expression is valid for nonrelativistic electron energies such that $\Delta E \ll mc^2$. Hence,

$$\Delta E \approx \frac{E_0^2}{mc^2}(1 - \cos\theta) - \frac{\hbar}{m} P \cdot \Delta k. \qquad (5.76)$$

The first term agrees with the usual expression for the Compton shift, (5.72), within the nonrelativistic approximation. The second term is a Doppler shift present because the scattering electron is in motion. Note that only the component of P in the direction Δk influences ΔE.

Equation (5.76) was derived for a fixed P; if there is a distribution in P, the scattered flux for a particular ΔE is given by

$$I(\Delta E) = \text{const.} \int_\infty d^3 P\, n(P) \delta\left[\Delta E - (\Delta E)_0 + \frac{\hbar}{m} P \cdot \Delta k\right], \qquad (5.77)$$

where

$$(\Delta E)_0 = \frac{E_0^2}{mc^2}(1 - \cos\theta). \qquad (5.78)$$

Equation (5.77) has the structure of a 3D Radon transform *in momentum space*. The usual parameters $\hat{n}$ and p are given by

$$\hat{n} = -\Delta k/|\Delta k|, \qquad (5.79)$$

$$p = \frac{m}{\hbar|\Delta k|}[\Delta E - (\Delta E)_0]. \qquad (5.80)$$

Hence, spectra taken at various scattering angles can be used to map out the full 3D Radon transform of $n(P)$. Some approximation to the inverse Radon transform can then be used to reconstruct $n(P)$ (MIJNARENDS [1977]).

A closely related technique that also measures $\mathscr{R}_3\{n(\boldsymbol{P})\}$ is positron annihilation (HAUTOJÄRVI [1979]; WEST [1974]).

An interesting mathematical point arises when Compton scattering or positron annihilation studies are carried out in oriented single crystals. Then it is convenient to use a spherical harmonic decomposition akin to (4.63), but with suitable linear combinations of spherical harmonics that reflect the symmetry of the crystal. These so-called lattice harmonics (MIJNARENDS [1967, 1977]) allow reasonable reconstructions of $n(\boldsymbol{P})$ from a relatively small number of points in Radon space.

5.7. MISCELLANEOUS APPLICATIONS

Many applications of the Radon transform to astronomy have been reported. Indeed, perhaps the first experimental implementation of the inverse Radon transform was the 1936 work of V. AMBARTSUMIAN, as reported by CORMACK [1982]. Ambartsumian examined the problem of deducing the 3D distribution of velocities of stars from measurements of doppler shifts, which are sensitive only to the radial component of velocity, and obtained a reconstruction of the velocity distribution projected on the galactic plane. BRACEWELL [1974] reviews many other astronomical applications, including strip-scan radio-astronomy, lunar occultation of radio sources, radar measurements of lunar roughness, and estimation of the density of globular clusters. ALTSCHULER and PERRY [1974] suggest 3D modeling of the solar corona, and the attenuated Radon transform could be applicable to solar limb darkening.

Another early application was to statistics. CRAMÉR and WOLD [1936] used the mD Radon transform to prove various theorems about mD probability distributions, using known results for 1D distributions.

Since the 1950s, there has been interest in optical computers for performing the inverse Radon transform. KORENBLYUM, TETEL'BAUM and TYUTIN [1958] designed an optical reconstruction system for medical CT, and the extensive work since then is reviewed by GMITRO, GREIVENKAMP, SWINDELL, BARRETT, CHIU and GORDON [1980]. One recent development is the application of optical Radon transformers to data-processing problems that initially do not involve projections at all (BARRETT [1982b, 1983]). Here the idea is to use the Radon transform as a pre-processing step to reduce 2D or 3D data sets to a series of more manageable 1D data sets.

Electron microscopy is another important application area. Here the main problem is that it is experimentally difficult to get a complete data set, and the

theoretical work is aimed at the ill-posed problem of reconstruction from incomplete projections.

This survey certainly does not exhaust the possibility applications of Radon theory. The proceedings of the Brookhaven (MARR [1974]) and Stanford (GORDON [1975]) conferences should be perused to gain a better impression of the richness of this field.

Acknowledgements

References

ABRAGAM, A., 1961, *The principles of Nuclear Magnetism* (Oxford University Press, London).

ALTSCHULER, M. S. and R. M. PERRY, 1974, The Three-dimensional Solar Corona, in: *Techniques of Three-dimensional Reconstruction*, Proc. Int. Workshop at Brookhaven Nat. Lab., ed. R. B. Marr (Brookhaven, Upton, LI).

ANGER, H. O., 1958, Scintillation Camera, Rev. Sci. Instrum. **29**, 27.

ANGER, H. O., 1964, Scintillation Camera with Multichannel Collimators, J. Nucl. Med. **5**, 515.

BARRETT, H. H., 1982a, Dipole-sheet Transform, J. Opt. Soc. Amer. **72**, 468.

BARRETT, H. H., 1982b, Optical Processing in Radon Space, Opt. Lett. **7**, 248.

BARRETT, H. H., 1983, Three-dimensional Image Reconstruction from Planar Projections, with Application to Optical Data Processing, in: *Transformations in Optical Signal Processing*, eds. W. T. Rhodes, J. R. Fienup and B. E. A. Saleh (S.P.I.E., Bellingham, WA).

BARRETT, H. H. and W. SWINDELL, 1981, *Radiological Imaging: Theory of Image Formation, Detection and Processing* (Academic, New York).

BELLINI, D., M. PIACENTINI, C. CAFFORIO and F. ROCCA, 1979, Compensation of Tissue Absorption in Emission Tomography, IEEE Trans. Acoust. Speech and Signal Process. **ASSP-27**, 213.

BOERNER, W.-M., 1979, Development of Physical Optics Inverse Scattering Techniques Using Radon Projection Theory, in: *Mathematical Methods and Applications of Scattering Theory*, Lecture Notes in Physics, vol. 130 (Springer, Berlin).

BOJARSKI, N. N., 1979, *N*-dimensional Fast Fourier Transform Tomography for Incomplete Information and Its Application to Inverse Scattering Theory, in: *Mathematical Methods and Applications of Scattering Theory*, Lecture Notes in Physics, vol. 130 (Springer, Berlin).

BRACEWELL, R. N., 1965, *The Fourier Transform and its Applications* (McGraw–Hill, New York).

BRACEWELL, R. N., 1974, Three-dimensional Reconstruction: An Overview, in: *Techniques of Three-dimensional Reconstruction*, Proc. Int. Workshop held at Brookhaven Nat. Lab., ed. R. B. Marr (Brookhaven, Upton, IL).

BROOKS, R. A. and G. DiCHIRO, 1976, Principles of Computer Assisted Tomography (CAT) in Radiographic and Radioisotopic Imaging, Phys. Med. Biol. **21**, 689.

BROWNELL, G. L., J. A. CORREIA and R. G. ZAMENHOF, 1978, Positron Instrumentation, Rec. Adv. Nucl. Med. **5**, 1.

BUDINGER, T. F. and G. T. GULLBERG, 1977, Transverse Section Reconstruction of Gamma-ray Emitting Radionuclides in Patients, in: *Reconstruction Tomography in Diagnostic Radiology and Nuclear Medicine*, eds. M. Ter-Pogossian et al.

CHAN, C. K. and N. H. FARHAT, 1981, Frequency Swept Tomographic Imaging of Three-dimensional Perfectly Conducting Objects, IEEE Trans. Antennas & Propag. **AP-29**, 312.

CHIU, M. Y., 1980, Three-dimensional Radiographic Imaging, Ph.D. Dissertation (Univ. of Arizona, Tucson).

CHIU, M. Y., H. H. BARRETT and R. G. SIMPSON, 1980. Three-dimensional Reconstruction from Planar Projections, J. Opt. Soc. Amer. **70**, 755.

CLOUGH, A. V. and H. H. BARRETT, 1983, The Attenuated Radon and Abel Transforms, J. Opt. Soc. Amer., to be published in November issue.

COMPTON, A. H., 1923a, The Spectrum of Scattered X-rays, Phys. Rev. **22**, 409.

COMPTON, A. H., 1923b, A Quantum Theory of the Scattering of X-rays by Light Elements, Phys. Rev. **21**, 207 and 483.

COMPTON, A. H., 1926, *X-rays and Electrons* (Van Nostrand, New York).

CORMACK, A. M., 1963, Representation of a Function by Its Line Integrals, with Some Radiological Applications, J. Appl. Phys. **34**, 2722.

CORMACK, A. M., 1964, Representation of a Function by Its Line Integrals, with Some Radiological Applications, II, J. Appl. Phys. **35**, 2908.

CORMACK, A. M., 1973, Reconstruction of Densities from Their Projections with Applications in Radiological Physics, Phys. Med. Biol. **18**, 195.

CORMACK, A. M., 1982, Computed Tomography: History and Some Recent Developments, Amer. Math. Soc. short course on computed tomography, Cincinnati, Jan. 1982.

COURANT, R. and D. HILBERT, 1962, *Methods of Mathematical Physics* (Wiley, London).

CRAMÉR, H. and H. WOLD, 1936, Some Theorems on Distribution Functions, J. Lond. Math. Soc. **11**, 290.

DÄNDLIKER, R. and K. WEISS, 1970, Reconstruction of the Three-dimensional Refractive Index from Scattered Waves, Opt. Commun. **1**, 323.

DAS, Y. and W. M. BOERNER, 1978, On Radar Target Shape Estimation Using Algorithm for Reconstruction from Projections, IEEE Trans. Antennas & Propag. **AP-26**, 274.

DEANS, S. R., 1978, A Unified Radon Inversion Formula, J. Math. Phys. **19**, 2346.

DEANS, S. R., 1983, *The Radon Transform and Some of its Applications* (Wiley, New York).

DEVANEY, A. J., 1980, Inverse Source and Scattering Problems in Optics, in: *Optics in 4 Dimensions*, eds. L. M. Narducci and M. A. Machado (AIP, New York).

DuMOND, J. W. M., 1929, Compton Modified Line Structure and Its Relation to the Electron Theory of Solid Bodies, Phys. Rev. **33**, 643.

DuMOND, J. W. M., 1933, The Linear Momenta of Electrons in Atoms and in Solid Bodies as Revealed by X-ray Scattering, Rev. Med. Phys. **5**, 1.

EIN-GAL, M., 1975, The Shadow Transform: An Approach to Cross-sectional Imaging, Ph.D. Dissertation (Stanford Univ.).

FARRAR, T. C. and E. D. BECKER, 1971, *Pulse and Fourier Transform NMR – Introduction to Theory and Methods* (Academic, New York).

FLORANCE, D. C. H., 1910, Primary and Secondary Gamma Rays, Phil. Mag. **20**, 921.

GASKILL, J. D., 1978, *Linear Systems, Fourier Transforms and Optics* (Wiley, New York).

GEL'FAND, I. M., M. I. GRAEV and N. YA. VILENKIN, 1966a, *Integral Geometry and Representation Theory* (Academic, New York).

GEL'FAND, I. M., M. I. GRAEV and N. YA. VILENKIN, 1966b, *Generalized Functions*, vol. 5 (Academic, New York), pp. 1–74.

GINDI, G. R., J. ARENDT, H. H. BARRETT, M. Y. CHIU, A. ERVIN, C. L. GILES, M. A. KUJOORY, E. L. MILLER and R. G. SIMPSON, 1982, Imaging with Rotating-Slit Apertures and Rotating Collimators, Med. Phys. **9**, 324.

GMITRO, A. F., J. E. GREIVENKAMP, W. SWINDELL, H. H. BARRETT, M. Y. CHIU and S. K. GORDON, 1980, Optical Computers for Reconstructing Objects from Their X-ray Projections, Opt. Eng. **19**, 260.

GORDON, R., ed., 1975, *Image Processing for 2-D and 3-D Reconstruction from Projections*, Proc. Symp. held at Stanford Univ., Aug. 4–7, 1975 (Optical Society of America, Washington).

GORDON, R., G. T. HERMAN and S. A. JOHNSON, 1975, Image Reconstruction from Projections, Scientific American, Oct., 56.

GRADSHTEYN, I. S. and I. M. RYZHIK, 1980, *Table of Integrals, Series, and Products* (Academic, New York).

GRAY, J. A., 1913, The Scattering and Absorption of the Rays of Radium, Phil. Mag. **26**, 611.

GULLBERG, G. T., 1979, The Attenuated Radon Transform: Theory and Application in Medicine and Biology, Ph.D. Thesis (Univ. of California, Berkeley).

HANSEN, E. W., 1981, Theory of Circular Harmonic Image Reconstruction, J. Opt. Soc. Amer. **71**, 304.

HAUTOJÄRVI, P., ed., 1979, *Positrons in Solids*, Topics in Current Physics, vol. 12 (Springer, Berlin).

HAWKINS, W., 1982, The Mathematics of Computed Tomography, Ph.D. dissertation (Univ. of Arizona, Tucson).

HELGASON, S., 1965, The Radon Transform on Euclidean Spaces, Compact Two-point Homogeneous Spaces and Grassmann Manifolds, Acta Math. **113**, 153.

HELGASON, S., 1980, *The Radon Transform* (Birkhäuser, Boston).

HERMAN, G. T., 1980, *Image Reconstruction from Projections* (Academic, New York).

HERMAN, G. T. and F. NATTERER, eds., 1981, *Mathematical Aspects of Computerized Tomography*, Lecture Notes in Medical Informatics, vol. 8 (Springer, Berlin).

JACKSON, J. D., 1975, *Classical Electrodynamics*, 2nd Ed. (Wiley, New York).

JASZCZAK, R., R. E. COLEMAN and C. B. LIM, 1980, SPECT: Single Photon Emission Computed Tomography, IEEE Trans. Nucl. Sci. **NS-27**, 1137.

JOHN, F., 1955, *Plane Waves and Spherical Means Applied to Partial Differential Equations* (Interscience, New York).

KAK, A. C., 1979, Computerized Tomography with X-ray, Emission, and Ultrasound Sources, Proc. IEEE **67**, 1245.

KARSTAEDT, N., R. L. WITCOFSKI and C. L. PARTAIN, 1981, eds., *Proc. Int. Symp. on NMR Imaging* (Bowman Gray School of Medicine Press).

KAUFMAN, L., L. E. CROOKS and A. R. MARGULIS, 1981, eds., *Nuclear Magnetic Resonance Imaging in Medicine* (Igaku–Shoin, Tokyo).

KENNAUGH, E. M. and D. L. MOFFATT, 1965, Transient and Impulse Response Approximations, Proc. IEEE **53**, 893.

KEYES, W. I., 1975, The Fan-beam Gamma Camera, Phys. Med. Biol. **20**, 489.

KORENBLYUM, B. I., S. I. TETEL'BAUM and A. A. TYUTIN, 1958, About One Scheme of Tomography, Izv. Vyschikh Uchebnykh Zavedenii-Radiofizika **1**, 151. (In Russian; English translation available from H. H. Barrett.)

LACOURT, A., J. C. VIENOT and J. P. GOEDGEBUER, 1976, Reassessing Basic Landmarks in Space–Time Optics, Opt. Commun. **19**, 68.

LAX, P. D. and R. S. PHILLIPS, 1967, *Scattering Theory* (Academic, New York).

LEWIS, R. M., 1969, Physical Optics Inverse Diffraction, IEEE Trans. Antennas & Propag. **AP-24,** 276.

LEWITT, R. M. and R. H. T. BATES, 1978, Image Reconstruction from Projections (Parts I–IV), Optik **50,** 19.

LIGHTHILL, M. J., 1962, *Fourier Analysis and Generalized Functions* (Cambridge University Press).

LINDGREN, A. G. and P. A. RATTEY, 1981, The Inverse Discrete Radon Transform with Applications to Tomographic Imaging Using Projection Data, in: *Advances in Electronics and Electron Physics*, vol. 56, ed. C. Marton (Academic, New York).

LUDWIG, D., 1966, The Radon Transform on Euclidean Space, Comm. Pure Appl. Math. **19,** 49.

MAGER, R. D. and N. BLEISTEIN, 1978, An Examination of the Limited Aperture Problem of Physical Optics Inverse Scattering, IEEE Trans. Antennas & Propag. **AP-26,** 695.

MANSFIELD, P. and P. G. MORRIS, 1982, *NMR Imaging in Biomedicine* (Academic, Cambridge).

MARR, R. B., ed., 1974, *Techniques of Three-dimensional Reconstruction*, Proc. Int. Workshop held at Brookhaven National Lab. (Brookhaven, Upton, LI).

MARR, R. B., C.-N. CHEN and P. C. LAUTERBUR, 1981, On Two Approaches to 3D Reconstruction in NMR Zeugmatography, in: *Mathematical Aspects of Computerized Tomography*, Lecture Notes in Medical Informatics, vol. 8, eds. G. T. Herman and F. Natterer (Springer, Berlin).

MIJNARENDS, P. E., 1967, Determination of Anisotropic Momentum Distributions in Positron Annihilation, Phys. Rev. **160,** 512.

MIJNARENDS, P. E., 1977, Reconstruction of Three-dimensional Distributions, in:*Compton Scattering*, ed. B. Williams (McGraw–Hill, New York) ch. 10.

MIJNARENDS, P. E., 1979, Electron Momentum Densities in Metals and Alloys, in: *Positrons in Solids*, ed. P. Hautojärvi (Springer, Berlin) ch. 2.

MORSE, P. M. and H. FESHBACH, 1953, *Methods of Theoretical Physics* (McGraw–Hill, New York).

PLATZMAN, P. and N. TZOAR, 1977, Theory, in: *Compton Scattering*, ed. B. Williams (McGraw–Hill, New York) ch. 2.

PYKETT, I. L., 1982, NMR Imaging in Medicine, Scientific American **246,** 78.

PYKETT, I. L., J. H. NEWHOUSE, F. S. BUONANNO, T. G. BRADY, M. R. GOLDMAN, J. P. KISTLER and G. M. POHOST, eds., 1982, *Principles of N.M.R. Imaging* **143,** 157.

RADON, J., 1917, Über die Bestimmung von Funktionen durch ihre Integralwerte längs gewisser Mannigfaltigkeiten, Ber. Saechs. Akad. Wiss. (Leipzig) **69,** 262.

RADULOVIC, P. T. and C. M. VEST, 1975, Direct Three-dimensional Reconstruction, in: *Image Reconstruction for 2-D and 3-D Reconstruction from Projections*, ed. R. Gordon (Digest of Technical Papers, Stanford, CA, Aug. 4–7, 1975).

ROCKMORE, A. G., R. V. DENTON and B. FRIEDLANDER, 1979, Direct Three-Dimensional Image Reconstruction, IEEE Trans. Antennas & Propag. **AP-26,** 274.

SHEPP, L. A., 1980, Computerized Tomography and Nuclear Magnetic Resonance, J. Comput. Assist. Tomog. **4,** 94.

SHEPP, L. A. and J. B. KRUSKAL, 1978, Computerized Tomography: the New Medical X-ray Technology, Amer. Math. Monthly **85,** 420.

SLICHTER, C. P., 1963, *Principles of Magnetic Resonance* (North-Holland, Amsterdam).

SMITH, K. T., D. C. SOLOMON and S. L. WAGNER, 1977, .Practical and Mathematical Aspects of the Problem of Reconstructing Objects from Radiographs, Bull. Amer. Math. Soc. **83,** 1227.

STEWART, A. T., 1957, Momentum Distribution of Metallic Electrons by Positron Annihilation, Can. J. Phys. **35,** 168.

STUEWER, R. H. and M. J. COOPER, 1977, History, in: *Compton Scattering*, ed. B. Williams (McGraw–Hill, New York) ch. 1.

SWINDELL, W. and H. H. BARRETT, 1977, Computerized Tomography: Taking Sectional X-rays, Physics Today **30,** 32.

TIPLER, P. A., 1969, *Foundations of Modern Physics* (Worth Publ., New York).

TRETIAK, O. J. and P. DELANEY, 1977, The Exponential Convolution Algorithm for Emission Computed Axial Tomography, in: *Information Processing in Medical Imaging* (Biomedical Computing Technology Information Center, Nashville, TN).

TRETIAK, O. J. and C. METZ, 1980, The Exponential Radon Transform, SIAM J. Appl. Math. **39**, 341.

VAN DER POL, B. and TH. J. WEIJERS, 1934, Tchebycheff Polynomials and Their Relation to Circular Functions, Bessel Functions and Lissajous Figures, Physica **1**, 78.

VERLY, J. G., 1981, Circular and Extended Circular Harmonic Transforms and Their Relevance to Image Reconstruction from Line Integrals, J. Opt. Soc. Amer. **71**, 825.

VEST, C. M. and D. G. STEEL, 1978, Reconstruction of Spherically Symmetric Objects from Slit-imaged Emission: Application to Spatially Resolved Spectroscopy, Opt. Lett. **3**, 54.

WEST, R. N., 1974, *Positron Studies of Condensed Matter* (Taylor and Francis, London).

WILLIAMS, B., ed., 1977, *Compton Scattering* (McGraw–Hill, New York).

WOLF, E., 1969, Three-dimensional Structure Determination of Semi-transparent Objects from Holographic Data, Opt. Commun. **1**, 153.

YOUNG, J. D., 1976, Radar Imaging from Ramp Response Signatures, IEEE Trans. Antennas & Propag. **AP-24**, 276.